Resumen

Los carburos cementados, materiales también conocidos por el nombre de metal duro, presentan excelentes propiedades tribomecánicas debido a la sinergia existente entre elevada dureza y rigidez aportadas por las partículas cerámicas y moderada, pero suficiente, tenacidad aportada por un aglomerante metálico. Debido a estas propiedades, los carburos cementados son ampliamente utilizados en diversas aplicaciones como componentes estructurales y materiales de herramientas. Sin embargo, en muchas ocasiones su empleo generalizado se ve limitado por la falta de información sobre la tolerancia al daño de dichos componentes y herramientas. Esto es particularmente cierto en el caso de las solicitaciones de contacto, uno de los modos de carga más comunes para las aplicaciones de metales duros.

El comportamiento mecánico de los carburos cementados ha sido ampliamente estudiado tomando en cuenta los defectos pre-existentes en el material (daños intrínsecos). Sin embargo, la información sobre los efectos del daño inducido en servicio (daños extrínsecos) en la integridad estructural de estos materiales es escasa.

El daño se puede introducir en materiales bajo solicitaciones de contacto, tanto monotónicas como cíclicas, mediante la técnica de indentación Hertziana. Para una carga umbral de indentación, se pueden generar dos típos de daño: aparición de grietas cónicas (comportamiento frágil) y deformación cuasi-plástica (comportamiento dúctil). Este trabajo tiene como objetivo el estudio de este daño inducido en metales duros, y las consecuencias del mismo en la resistencia mecánica del material. Para ello, se observa la evolución del daño inducido por contacto, tanto en la superficie como en la sub-superficie de los materiales, previamente a la evaluación de la resistencia residual de fractura. El trabajo se lleva a cabo en dos calidades de metales duros de microestructura diferente (grano fino y submicrométrico) con la idea de poder evaluar la influencia de la microestructura en el comportamiento mecánico de estos materiales.

Se estableció que al incrementar el tamaño de grano del carburo y el contenido de cobalto, el comportamiento del metal duro frente a la indentación esférica, tanto con cargas monotónicas como cíclicas, es cada vez más cuasi-plástico. Materiales de comportamiento exclusivamente cuasi-plástico sufren una degradación de resistencia gradual y suave a medida que aumenta la carga monotónica. En fatiga, la degradación es aún menos pronunciada, reflejando así la relativamente alta tolerancia al daño de estos materiales. Sin embargo, la pérdida de resistencia aumenta a 10^6 ciclos, debido a la formación de grietas radiales, indicando una susceptibilidad de acumulación de microdaño en el material.

El material más duro sufre un estado de daño mixto con aparición de grietas cónicas (para cargas monotónicas elevadas y, en fatiga, para números de ciclos bajos) y deformación cuasi-plástica. Se sospecha que la aparición de grietas cónicas causa una caída en la resistencia mecánica, efectivamente observada para la carga crítica bajo solicitaciones monotónicas, igual que para un número de ciclos bajo. Sin embargo, al extenderse las zonas cuasi-plásticas (en fatiga, para números de ciclos altos), los mismos pueden interactuar con la fisura cónica para neutralizar su efecto dañoso, de manera que la resistencia mecánica se recupera.

Abstract

Cemented carbides, materials also known as hardmetals, present excellent tribomechanical properties due to the synergy existing between the elevated hardness, provided by ceramic particles, and moderate but sufficient toughness, contributed by a metallic binder. These properties are responsible for the extensive use of cemented carbides in structural and tooling applications. However, the use of the mentioned components and tools are somewhat limited due to a lack of information on the mechanical reliability of these materials. This is particularly true for the case of contact loading, one of the most common loading modes existing within hardmetal application.

The mechanical behavior of the cemented carbides has been thoroughly studied taking into account pre-existing material defects introduced from processing (intrinsic damage). However, the information about the effects of damage induced during service (extrinsic damage) on structural integrity of these materials is scarce.

Damage can be induced into the materials by means of applied contact loading, with monotonic as well as cyclic load levels, using the Hertzian indentation technique. At a certain critical load, this spherical contact can generate two types of damage: cone cracking (brittle response) and quasi-plastic deformation (ductile response). This project aims to study such induced damage in hardmetals, and its consequences in the mechanical strength of the material. In doing so, evolution of the contact induced damage was observed from surface and cross-sectional viewpoints, prior to the evaluation of residual flexural strength. The study is carried out in two microstructurally different grades of cemented carbides (fine and submicron grain size) with the purpose of evaluating the influence of microstructure on the mechanical behavior of these materials.

It was found that as carbide grain size and metallic binder content increase, the hardmetal response to spherical indentation, under monotonic as well as cyclic loading, is increasingly quasi-plastic. Materials with exclusively quasi-plastic behavior experience minor gradual strength degradation as monotonic load levels increase. In fatigue, degradation is even less important, reflecting the relatively high damage tolerance of these materials. However, an increased loss in strength is noted at $n = 10^6$ cycles, related to the formation of radial cracks, pointing out then the susceptibility of the material to microdamage accumulation.

The harder material experiences a mixed damage mode with formation of both cone cracks (at elevated monotonic load levels and, in fatigue, from small numbers of cycles) and quasi-plastic zones. Cone crack formation is suspected to cause a drop in fracture strength, effectively occurring at the critical monotonic load level, as well as at small numbers of cycles. However, as the quasi-plastic zones extend (i.e. at high cyclic loading), these may interact with cone cracks and neutralize their deleterious effects, providing hence a recovery in mechanical fracture strength.

Table of contents

1. Introduction

1.1 Cemented carbides

Cemented carbides are wear-resistant, refractory materials made up of small carbide particles embedded in a metallic phase usually consisting of cobalt. It is hence a ceramic-metal composite whose composition varies with application purpose, usually having a 70-95% content of carbide and 30-5% content of metallic binder. This structure combines the hardness and wear resistance of the ceramic particles with the toughness of the metallic binder, giving the material a unique combination of strength, hardness, toughness and wear resistance. As a consequence, they have proved to be first-choice materials in engineering and tooling applications, such as metal cutting, mining, rock drilling, metal forming, structural components and wear parts.

1.1.1. Composition and applications

The original cemented carbide consisted of tungsten carbide particles bonded together by cobalt. Cobalt has great wetting and adhesion characteristics and is thus the preferred binder of the carbides, making this original composition highly essential even to today's date. Even so, other types of cemented carbides have been developed throughout the years, designed to enhance certain properties of the original material. For example, nickel can be used as metallic binder, though the alloy corresponds to less than 10% of the total cemented carbide production. This change of binding element causes a fall in hardness and toughness for equal binder contents, but does provide an enhancement in corrosion and oxidation resistance.

Furthermore, the ceramic particle can be partly replaced by other carbides, such as titanium-, tantalum-, niobium-, vanadium-, hafnium-, molybdenum-, and zirconium carbides. Adding these carbides to the material leads to a decrease in the susceptibility to chemical attack and diffusion wear when cutting steels. This has allowed for an extended use of these alloys as steel-cutting tools, and they are generally referred to as Cermets, from CER(amic) + MET(al).

The microstructure of cermets contains three phases: angular tungsten carbide grains, rounded WC-TiC-(Ta,Nb)C solid-solution grains, and cobalt binder. Properties vary greatly with size, content and distribution of these phases.

Straight tungsten carbide-cobalt alloys (WC-Co) contain generally 3-25% per weight cobalt and the tungsten carbide particles vary in size from 0.5 to 30 µm. Ideally, they consist thus of two phases: angular tungsten carbide (WC) grains and the cobalt binder phase. Nevertheless, in order to achieve this composition a great deal of attention needs to be paid to the carbon content of the carbide. If it exceeds a certain quantity, free and finely divided graphite can take form, which could lead to unwanted effects in machining applications. On the other hand, a lack in carbon gives rise to a η phase consisting of a series of double carbides, causing severe embrittlement.

By altering the carbide and metal contents as well as the particle size of the tungsten carbide various grades of cemented carbides can be obtained. Properties depend greatly on both of these factors, giving the material a large property span. This is illustrated in Figure 1.1(a), which also places the properties of cemented carbides relative to other hard engineering materials.

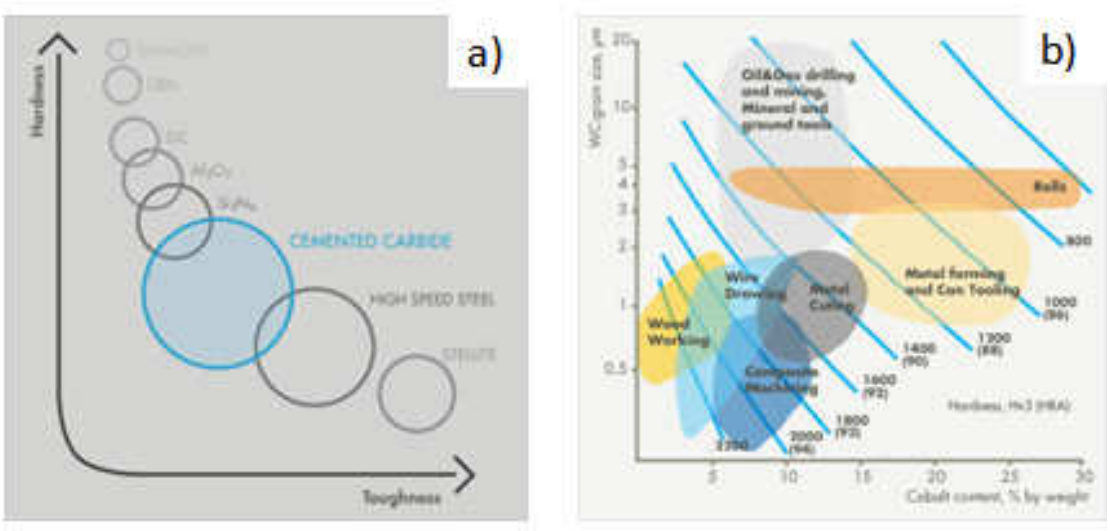

Figure 1.1. Property and application ranges of cemented carbides with (a) hardness and toughness span relative to other hard materials, and (b) carbide grain size as a function of cobalt content, displaying hardness values as blue lines. [9]

With the tungsten carbide size variations ranging from 0.5 to 30 µm, cemented carbides of nano- to extra-coarse grades can be obtained. Figure 1.2 shows typical microstructures of several of these grades.

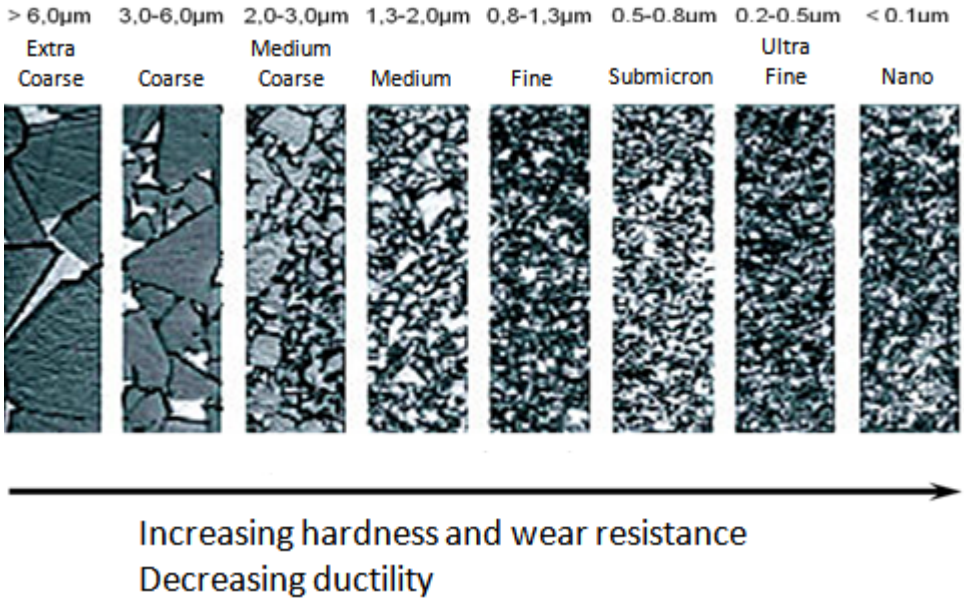

Figure 1.2. Microstructures of cemented carbides with carbide grain sizes ranging from nanoscopic to extra coarse.

Coarser grades present good combinations of high strength, toughness and abrasive wear resistance; thus, they are used in oil, gas and mining applications. On the other hand, the finer grades are used in a variety of solid carbide drilling and milling tools – applications requiring superior hardness and edge strength. The latter are very hard, extremely wear resistant and have high compressive strength. Figure 1.1(b) presents a chart of the many application fields of cemented carbides as a function of different binder content and tungsten carbide grain size.

1.1.2. Properties

As mentioned earlier, the carbide particles of hard metals provide hardness whereas the metallic binder adds toughness to the material. Thereby, with decreasing cobalt content and tungsten carbide grain size, properties like hardness, abrasion resistance, density and compressive strength of the cemented carbides increase (Figure 1.3). In most tooling and machining applications the materials have to endure high temperatures. As expected, hardness and compressive strength decrease as temperature increases. Moreover, although fine-grain carbides possess superior strength at room temperature, they present a faster drop in yield strength with increasing temperature.

The modulus of elasticity increases with decreasing cobalt content but is independent of carbide grain size. It is worth mentioning that apart from diamond and cubic boron nitride,

cemented tungsten carbides have the highest modulus of elasticity of all commercially available materials.

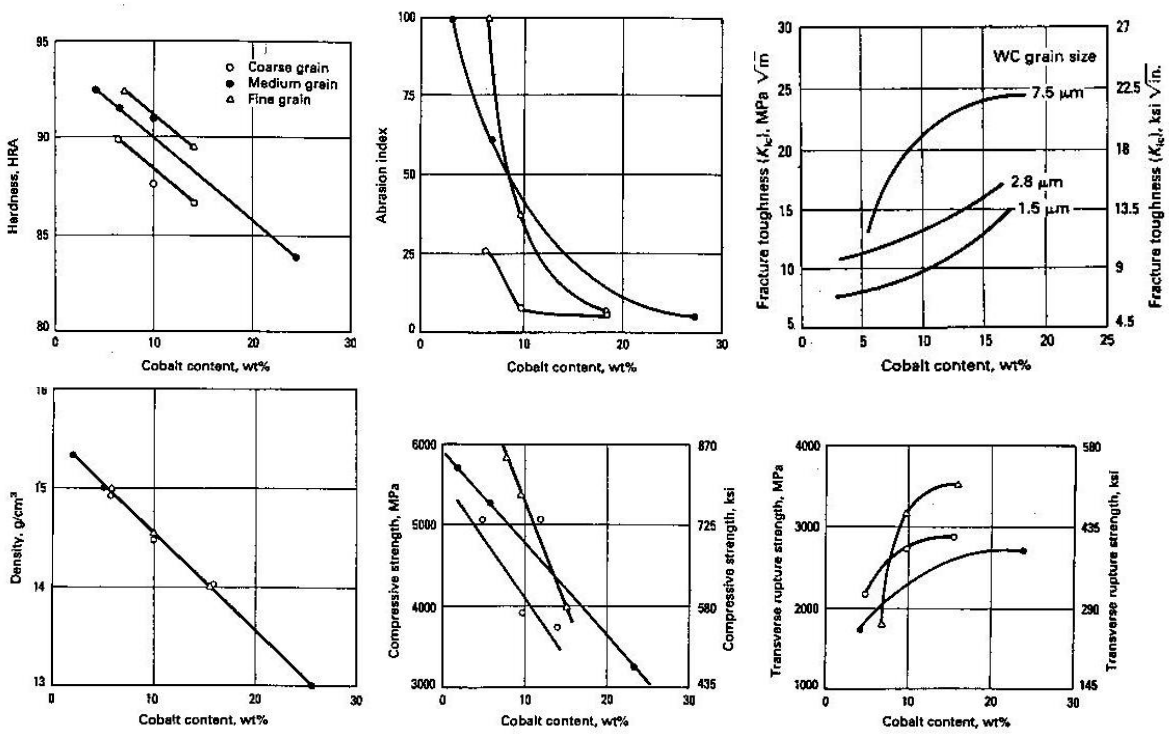

Figure 1.3. Hardness, abrasion index, fracture toughness, density, compression strength and transverse rupture strength as a function of cobalt content in cemented carbides. [8]

Contrary to the properties mentioned, increasing cobalt content provides higher fracture toughness and transverse rupture strength (Figure 1.3). Fracture toughness also increases with tungsten carbide grain size and temperature. Table 1.1 displays typical property values of some straight graded cemented tungsten carbides.

Table 1.1. Properties of representative cobalt-bonded cemented carbides. [8]

Nominal composition	Grain size	Hardness, HRA	Density g/cm³	Transverse strength MPa	Compressive strength MPa	Modulus of elasticity GPa	Relative abrasion resistance (a)
97WC-3Co	Medium	92.5-93.2	15.3	1590	5860	641	100
94WC-6Co	Fine	92.5-93.1	15.0	1790	5930	614	100
	Medium	91.7-92.2	15.0	2000	5450	648	58
	Coarse	90.5-91.5	15.0	2210	5170	641	25
90WC-10Co	Fine	90.7-91.3	14.6	3100	5170	620	22
	Coarse	87.4-88.2	14.5	2760	4000	552	7
84WC-16Co	Fine	89	13.9	3380	4070	524	5
	Coarse	86.0-87.5	13.9	2900	3860	524	5
75WC-25Co	Medium	83-85	13.0	2550	3100	483	3
71WC-12.5TiC-12TaC-4.5Co	Medium	92.1-92.8	12.0	1380	5790	565	11
72WC-8TiC-11.5TaC-8.5Co	Medium	90.7-91.5	12.6	1720	5170	558	13

(a) Based on a value of 100 for the most abraison-resistant material

Apart from the mechanical properties, cemented carbides also exhibit interesting magnetic, electric and thermal properties. Due to the ferromagnetic nature of cobalt, the cemented carbides display some magnetic saturation, this being larger as cobalt content increases. Additionally, cemented carbides may be described as electrical and thermal conductive materials. The latter is highly necessary in machining applications in order for the tool to conduct heat away from the tool/work piece interface. In hardmetals, thermal conductivity increases with decreasing cobalt content and rests unaffected by carbide grain size. On the contrary, the coefficient of thermal expansion increases with cobalt content.

Finally, the corrosion resistance of straight grades of cemented carbides is inversely related to the cobalt content. In fact, it is much dependent on the susceptibility of the cobalt binder to chemical attack, in which case the binder is dissolved leaving behind only the tungsten carbide particles that are then easily abraded away. Because the corrosion resistance of cobalt-base grades is not noticeable, it has been enhanced by introducing nickel binder grades alloyed with chromium, molybdenum and other elements.

1.1.3. Fabrication

Cemented carbides are produced by powder metallurgy. Accordingly, the tungsten carbide powder is mixed with the cobalt powder to fulfill the reached-for composition. The mixture is compacted into a form and undergoes a high-temperature sintering process including removal of lubricants, densification and microstructure development, reaching temperatures up to 1500

°C. This process causes shrinkage of about 50% in volume and determines the final form of the carbide. Finishing processes are grinding, lapping and polishing.

One of the drawbacks of cemented carbides is their relatively brittle nature. This means that the material is sensitive to flaws and damage within the material; thus, crack propagation, when started, can take place very fast leading to devastating consequences. It is therefore of much interest to study up to which extent cemented carbides are damage tolerant and how this tolerance is affected while the material is in use, i.e. whilst damage may be induced in the material under service conditions.

The present study focuses on this aspect and attempts to evaluate how the properties of cemented carbides are affected by the presence of damage in the material. In order to asses such damage tolerance, Hertzian contact tests, under monotonic and cyclic loading conditions, were performed by means of spherical indentation. The test method was chosen because of its proven utility in similar studies mainly on ceramics [1, 4, 6], but also on cemented carbides [3, 5, 10, 12]. In the following section, this test technique will be thoroughly described.

1.2 Spherical indentation

Spherical indentation is a contact test technique where hard spheres are used to introduce controlled damage into a given material such to evaluate its deformation and fracture properties. Additional mechanical properties that may be assessed are yield strength, toughness and wear. These tests are also usually referred to as Hertzian indentation tests after the pioneering work conducted by Heinrich Rudolf Hertz, a German physicist who first investigated contact stresses and contact related fracture mechanisms of glass lenses.

The Hertzian indentation technique consists in applying load onto the surface of the studied material using rigid spheres. The interaction between the sphere and the surface leads to elastic or fully plastic deformation depending on the load applied. In this way, the entire evolution of damage modes can be observed; within both elastic and elastic-plastic regimes.

Two types of fractures are generally produced by the spherical indentation method and these are often referred to as Hertzian fractures. In brittle materials the fracture adopts the shape of

a cone, nucleating as a ring crack on the border of the indentation mark and at a critical load propagating downwards and outward into the cone shape. Materials with superior fracture toughness will rather be affected in the area directly below the indentation which, upon contact loading, can turn into a "quasi-plastically deformed" zone. These damage modes will be described further in section 1.2.2.

Starting off by investigating flat silicate glass plates, the Hertzian fracture studies have extended its use to other brittle solids, particularly single crystals and some hard, fine-grain polycrystalline ceramics. In the last two decades, such experimental approach has also been employed for studying the mechanical contact response of heterogeneous ceramics with weak internal interfaces, large and elongated grains, and high internal residual stresses [1].

1.2.1 Contact stress fields

In Hertzian indentation tests the frictionless contact of a sphere of radius *r* at normal load *P* on a flat continuum specimen is considered (Figure 1.4). Hence, it is assumed that there is no relative motion between the two surfaces.

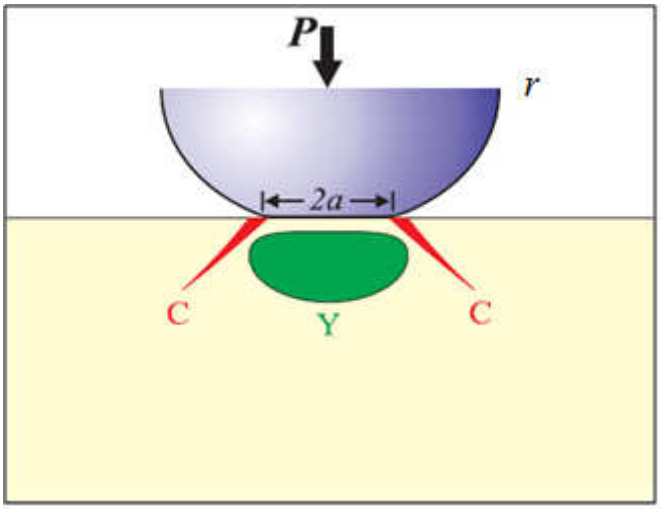

Figure 1.4. Illustration of the Hertzian contact with load *P*, contact radius *a*, and indenter radius *r*. The colored zones C (red) and Y (green) indicate location of the two types of fractures generated in materials through contact tests. [2]

When the material under consideration is first loaded, the underlying stress field is elastic. As the load increases to a certain point plastic flow will occur beneath the contact area. The local deformations produced by this contact were estimated by Hertz considering the two bodies as being semi-infinite elastic solids with an applied pressure evenly distributed over its circular

contact area (Figure 1.5). In order for this assumption to be valid, two conditions must be fulfilled:

- The contact area must be small in comparison to the dimensions of the two bodies.
- The radius of the contact area, *a*, needs to be considerably smaller than the radius of the sphere, *r*. In this way, the contact surface can be considered flat and the deformations very small, including exclusively elastic. [2]

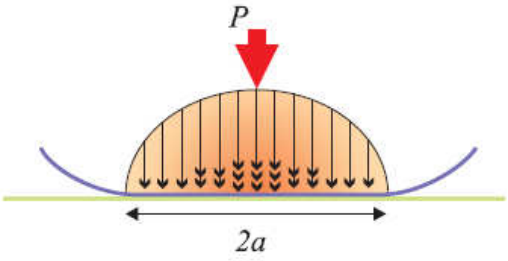

Figure 1.5. Distribution of the applied load during Hertzian contact. [2]

Hertzian theory includes two types of contact stress fields, associated with the elastic and elastic-plastic contacts respectively.

The elastic stress fields explored by Hertz originate in the calculation of the contact radius, i.e. the common radius of the indenter and the material under contact. When a sphere of radius *r* with the applied load *P* is put in contact with a specimen, the contact radius *a* is given by

$$a^3 = \frac{4kPr}{3E} \tag{1}$$

where *E* is Young´s modulus of the specimen and *k* is a dimensionless constant given by

$$k = \frac{9}{16}\left[(1-\nu^2) + (1-\nu'^2)\frac{E}{E'}\right] \tag{2}$$

with ν Poisson's ratio of the specimen and the prime notation indicating the properties of the indenter material. This radius defines the spatial scale of the contact field [1]. The intensity of the same is defined by the mean contact pressure, being

$$p_0 = \frac{P}{\pi a^2} \tag{3}$$

By combining Equations (1) and (3) the mean contact pressure ("indentation stress") can be expressed as a function of deformation *a/r* ("indentation strain") as follows:

$$p_0 = \left(\frac{3E}{4\pi k}\right)\frac{a}{r} \tag{4}$$

The maximum tensile stress in the specimen is located at the contact circle whereas the maximum shear stress occurs along the contact axis at a depth ≈0.5*a* below the surface. These stresses can be calculated as follows:

$$\sigma_m = \frac{1}{2}(1-2\nu)p_0 \tag{5}$$

$$\tau_m = 0.48p_0 \tag{6}$$

The principal stresses within the Hertzian elastic contact field are calculated using cylindrical coordinates, taking *z* to be in the same direction as the axis of applied load, as shown in the literature [1, 2]. The following relation is defined: $\sigma_1 \geq \sigma_2 \geq \sigma_3$ in all parts of the specimen, except for in a small region close to the surface and right beneath the contact zone where $\sigma_3 > \sigma_2$. The most tensile principal stress throughout the specimen remains being σ_1. The maximum principal shear stress is $\tau_{13} = \frac{1}{2}(\sigma_1 - \sigma_3)$ and is located at a depth ~*0.*5a beneath the contact surface.

Figure 1.6 shows the contours of the principal normal and shear stresses. Regions that are under tensile and shear stresses are shown in color, and are to be highlighted as these are the forces responsible for the inelastic response of the indented material to the contact. This response is to be more thoroughly explained further on.

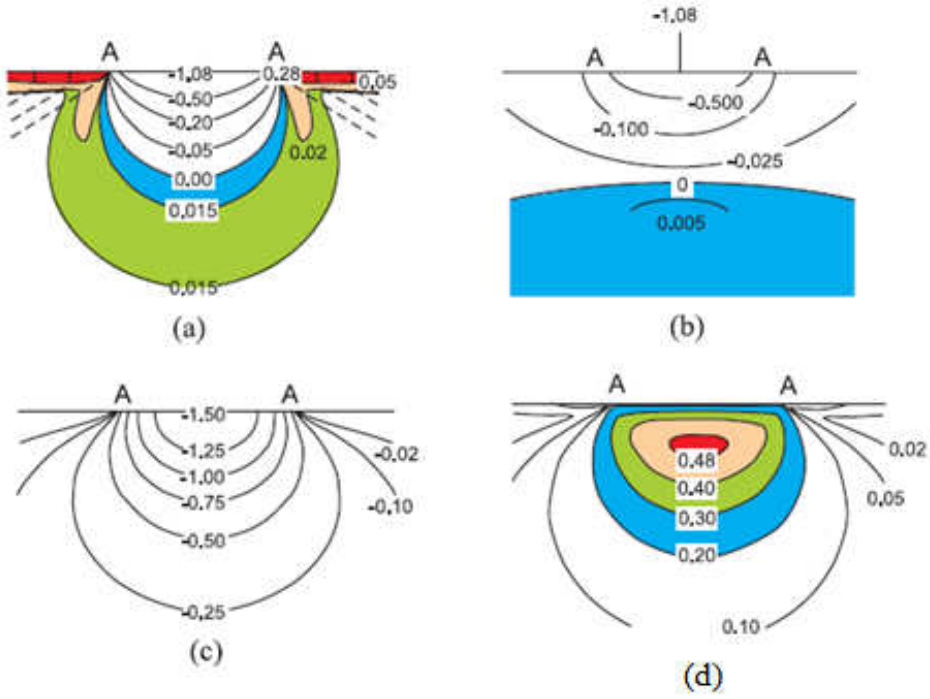

Figure 1.6. Principal stresses in the Hertzian contact field: (a) maximal principal normal stress, σ_1, (b) principal normal stress, σ_2, (c) minimal principal normal stress, σ_3, (d) maximal principal shear stress, τ_{13}. [2]

It is demonstrated in Figure 1.6(a) that principal tensile stresses are concentrated within a small shallow area close to the surface and reach a maximum value at the contact circle. The principal shear stresses shown in Figure 1.6(d), exhibit important values and are spread in the region beneath the contact, with a maximum value in the same direction as the contact axis.

To follow the transition from elastic to plastic contacts in hard materials, indentation stress-strain curves have proven to be useful. Plotting Equation (4) in a graph gives the elastic response to Hertzian contact. However, when introducing measured values of the indentation stress and strain, the indentation curve can deviate from the linear relationship indicating that the material is undergoing some plastic deformation [1, 11]. This behavior is observed for hardmetals as demonstrated in Figure 1.7, which shows an indentation stress-strain curve of a cemented tungsten carbide with a 10wt% content of cobalt [3]. The dashed line describes the Hertzian elastic behavior as defined by Equation (4).

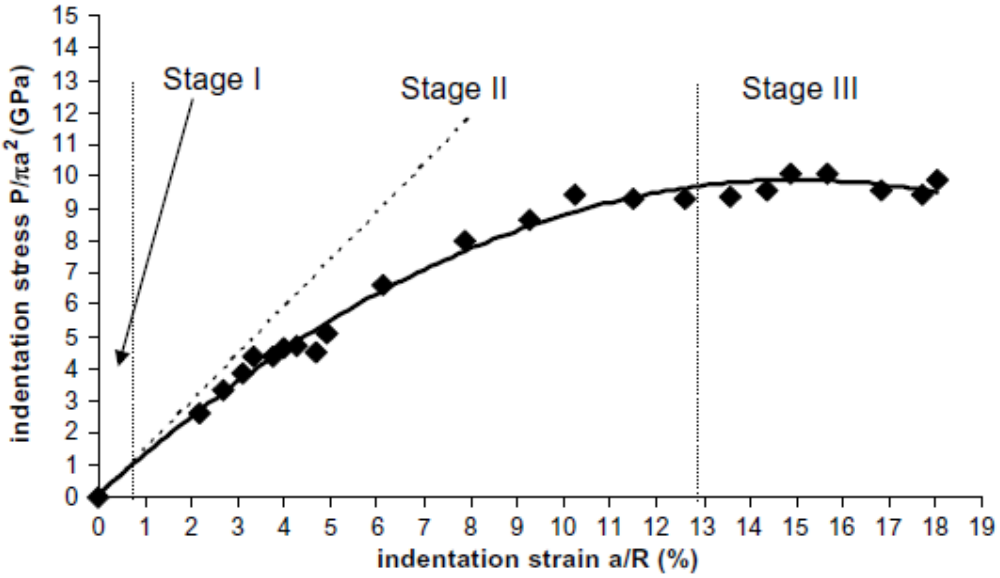

Figure 1.7. Indentation stress-strain curve for a WC-10wt%Co. The dashed line corresponds to the linear elastic response as defined by Hertz. [3]

Figure 1.7 indicates three regimes separating the different mechanisms that occur during the process from deformation to fracture. At stage I the curve is linear and follows the Hertz relation by Equation (4), thus the material's response to the contact is elastic. A yielding behavior is observed commencing at stage II and as a consequence, a yield point can be defined above which the indentation stress continues to increase monotonically with indentation strain, exhibiting an "apparent strain hardening" behavior [3].

The yielding point, hence obtained experimentally, allows for further property recognition. In accordance with Equation (6) the maximal shear stress is equal to $\tau_m = 0.48p_0$, and logically the plastic deformation occurs when this stress reaches a certain critical value. The two principal criteria of plasticity, being those of Tresca and Von Mises, both predict plastic flow to occur when

$$\tau_m = \frac{Y}{2} \tag{7}$$

where Y is the uniaxial compression yield stress. Combining these two equations allows for the following expression of the contact stress critical for initiation of plasticity:

$$p_Y \approx 1.1Y \tag{8}$$

Using this expression, the Hertzian indentation technique provides a means of evaluating the uniaxial compression yield stress.

No analytical model exists that fully describes the indentation stress-strain response in hard materials such as ceramics and cemented carbides. In consequence, finite-element modeling (FEM) is used for numerical modeling of the contact process, including the elastic-plastic and plastic response. Here, a yield condition is introduced into the FEM algorithm, together with a bilinear stress-strain curve $\sigma(\varepsilon)$ in ideal uniaxial compression for both the specimen and the indenter material:

$$\sigma = E\varepsilon \qquad (\sigma \leq Y) \tag{9a}$$

$$\sigma = Y + \alpha(\varepsilon E - Y) \qquad (\sigma \geq Y) \tag{9b}$$

where E is Young's modulus, Y is the uniaxial yield stress, and α is a dimensionless coefficient indicating the level of strain-hardening with the range $0 \leq \alpha \leq 1$. At $\alpha = 0$ the contact is fully plastic and at $\alpha = 1$ fully elastic [1].

The mentioned strain hardening has been studied in ceramic materials with quasi-plastic deformation and was correlated with microcracking as follows [3].

$$\alpha = \frac{1}{1 + 2Nl^3} \tag{10}$$

with N the number density and l the size of the microcrack. Here, limits are $2Nl^3 \ll 1$ corresponding to a fully elastic response and $2Nl^3 \gg 1$ to a fully plastic response. This correlation permits the incorporation of microstructural variables into the analysis of indentation stress and strain.

In conclusion, it is evident that the Hertzian indentation technique provides a good, versatile method for the mechanical characterization of a large variety of materials. The ability to control the applied loads, such to cause both reversible and irreversible deformations to the material, allows one to obtain a complete stress-strain curve. In addition, the tests enable the evaluation of the material's elastic (E) and plastic properties (Y), as well as the study of the different contact damage modes generated in the material tested.

1.2.2 Damage modes

As mentioned earlier, the Hertzian contact technique can generate two different damage mechanisms in the material; cone fracture (brittle mode) and quasi-plastic deformation (ductile mode). The presence and extension of each mode in a tested material depends on the nature of this material.

Relatively hard, homogeneous materials such as glasses, single crystal, and fine-grained ceramics when tested under spherical indentation tend to respond in a purely brittle manner. On the other hand, tougher ceramics with heterogeneous microstructures present what is called “quasi-plastic” damage upon indentation testing. In some hard materials both of these damage modes will be present when they are subjected to contact stresses. This is the case for cemented carbides.

Cone Fracture in Brittle Solids

Cone cracks nucleate from flaws on the specimen top surface at the contact circle where the tensile stresses are concentrated. The small cracks encircle the contact region forming a shallow annular fissure which then propagates downward and outward, generally following the σ_3 trajectories shown in Figure 1.8.

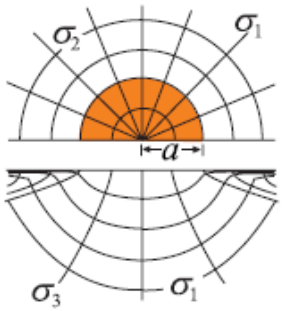

Figure 1.8. Principal stress trajectories generated by Hertzian contact loading at the surface (top) and in the section (bottom) of the specimen. The colored region corresponds to the area in contact. [2]

Figure 1.9 shows a good example of the appearance of cone fracture, seen from above and from a cross-sectional view.

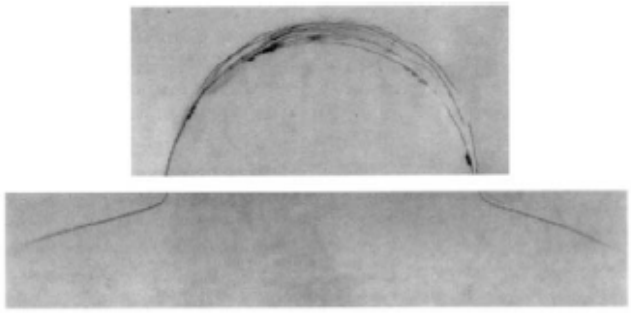

Figure 1.9. Micrographs of a cone crack in silicon nitride, product of Hertzian contact, that shows the surface (top) and cross-sectional (bottom) view of the specimen. [2]

Due to the rapid decrease of σ_1 as the distance to the contact surface grows, the downward propagation of the crack is impeded. The cone crack can therefore be considered a stable fissure. If the material is further loaded when the cone crack has reached the full lap around the contact circle, the annular crack will multiply and new circular fissures will be observed on the outside of the first crack.

The critical load at which cone cracks start nucleation and, further on, propagation has been thoroughly studied during many years and the results of this research are, still to this day, somewhat contradictory. Already in 1891 an empirical law was defined by Auerbach that related the critical contact load for initiating cone cracks to the radius of the indentation sphere as $P_C \propto r$. This law was adjusted by Tillett who proved the existence of two regions: the Auerbach region corresponding to small r where $P_C \propto r$, and a second region in which the curve divert from this dependency and tend to fall in parallel with the asymptote $P_C \propto r^2$ (Figure 1.10).

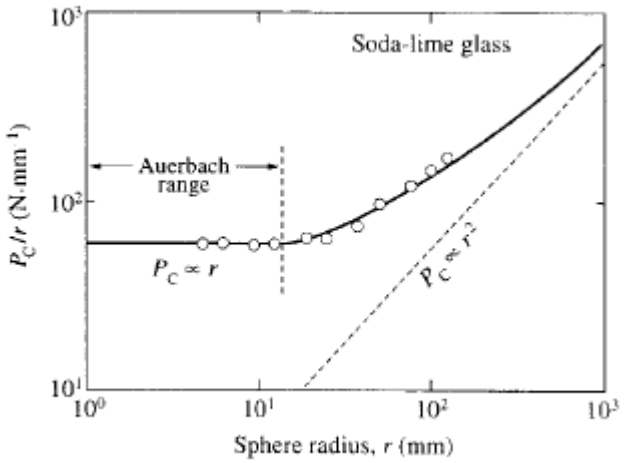

Figure 1.10. Experimental critical load for cone crack initiation as a function of indenter radius for polished soda-lime glass. The dashed line corresponds to the behavior predicted by equation (10). [2]

It is logical to suggest that the initiation of a crack is to start when the load generates tensile stresses in the contact region that exceed the fracture strength of the material ($\sigma_m \geq \sigma_F$). Considering this statement, the following expression of critical load is obtained:

$$P_C = \frac{9}{128}\frac{[\pi(1-2\nu)\sigma_F]^3}{E^{*2}}r^2 \tag{11}$$

derived from the expressions of the maximal tensile stress (Equation (5)) and the mean contact load;

$$p_0 = \frac{P}{\pi a^2} = \frac{2}{3}p_{max} = \left(\frac{16PE^{*2}}{9\pi^3 r^2}\right)^{1/3} \tag{12}$$

where E^* is the effective Young's modulus given by

$$\frac{1}{E^*} = \frac{1-\nu^2}{E} + \frac{1-\nu'^2}{E'} \tag{13}$$

with the prime notation corresponding to the properties of the indenter material.

According to Equation (11), the critical load is proportional to the radius of the indenter sphere as $P_C \propto r^2$. Experimentally though, this relation fails to prove its point for spheres with smaller radius when in fact, the values of the critical load calculated with this expression are much smaller than those obtained experimentally.

Another expression of the critical load as a function of sphere radius valid for small *r* was suggested by Frank and Lawn in 1967, derived from Auerbach's law. They used the fracture theory of Griffith-Irwin, suggesting there should be a critical crack length, c^*, below which the surface flaws develop in a very complex yet stable manner and at which the actual full cone crack pops in. This discovery renders P_C independent of the precursor flaw size in the Auerbach region, and proposes that the actual critical condition for cone crack initiation is when the stress-intensity factor, *KI*, is equal to the toughness of the material, *T*, taking this to be constant ($K(c) = T$) and $\frac{dK}{dc} > 0$. Using this criterion, the following expression is obtained cone crack initiation:

$$P_C = \theta \frac{T^2}{E^*} r \tag{14}$$

where $\theta = \theta(\nu)$, a dimensionless parameter that can be calculated experimentally [2]. Equation (14) is simply a formal statement of Auerbach's law.

The indenters used for the Hertzian contact technique are usually of small sphere radius, corresponding to the Auerbach region. Under these conditions, Equation (14) is used to evaluate critical contact loads for cone crack initiation [2].

It is worth mentioning that cone cracks in brittle materials seldom lead to fracture of the material thanks to its stable nature. Nonetheless, it affects the materials' properties, especially under fatigue loading and in water or other aggressive environments due to slow propagation of the crack. Under extreme conditions, the accumulation of this type of brittle damage can lead to material extraction on the surface of the same [2].

For materials with more heterogeneous microstructures and thus, a more ductile behavior, the damage mode is fundamentally different, as will be described now.

Quasi-Plastic Damage

Upon loading a relatively tough ceramic with heterogeneous microstructure, a first response to the contact will be a visible "sink-in"-impression on the material's surface. The underlying damage can be observed using a split-and-bond specimen (see section 3.2.3.), making possible a cross-sectional view of the material. In Figure 1.11, a micrograph of such a specimen having undergone quasi-plastic damage is shown.

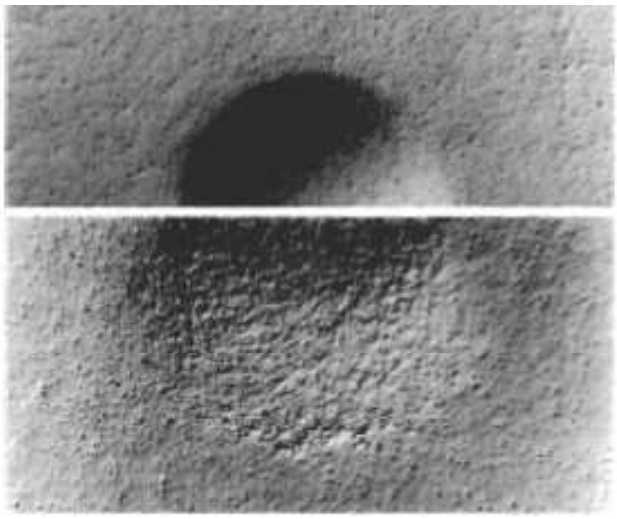

Figure 1.11. Half –surface (top) and cross-section (bottom) of a partially crystallized ceramic-glass presenting quasi-plastic deformation. [4]

Shear stresses are responsible for the generation of this damage, which develops in a region of hemispherical shape right beneath the contact zone. It is in this zone that the shear stresses, τ_{13}, attain their maximum values (Figure 1.6).

The evolution of the subsurface damage due to increased applied contact loading can be modeled. It is shown in Figure 1.12, where the A indicates the outer limits of the contact circle. The model confirms that the deformation first occurs in a zone parallel to the contact axis at a depth of 0.5*a* below the top surface, earlier defined as the region of maximal shear stress. As it can be observed, the deformed area expands upon increasing load to the sides and downward into the specimen, but very little towards the surface. Under a certain amount of load, the deformation reaches the top surface with the lateral walls touching the outer limits of the contact circle. From here on, the deformed zone spreads in areas far from the contact region, finally giving rise to the characteristic shape of a kettle.

No or little cone cracking is observed during this process. Due to the heterogeneous microstructure of the material in which the process takes place, the annular fissures deflect along the weak interfaces, away from the strongly tensile zones and into regions that lie under compressive stresses where the fissure is suppressed.

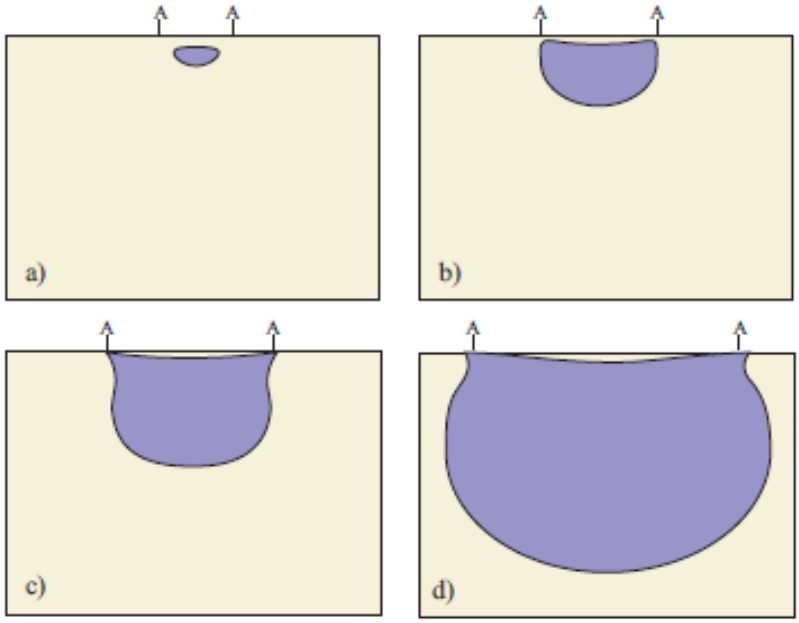

Figure 1.12. Schematic evolution of the quasi-plastic damage occurring under Hertzian contact tests with increasing load. The outer contact limits are indicated with an A. [2]

The quasi-plastic zone in ceramics is macroscopically similar to the yield zones generated by hardness tests in soft metals. However, a closer look shows a much more highly constrained state beneath the contact in the quasi-plastic zone, and the two materials undergo completely different micromechanisms.

While typical mechanisms of deformation in metals include dislocation movement and twinning, the quasi-plastic zones consist of distributed shear-fault microfailures that occur at the weak interfaces within the material in question (in cemented carbides, these weak interfaces give way to microcracking along several crack paths in the microstructure: transgranular cracks through WC grains, intergranular cracks along WC/WC grain boundaries, and cracks along the WC/Co interfaces [3]). The shear faults may in turn initiate secondary microcracks at their ends, especially where the faults intersect with weak grain or interphase boundaries [1].

Figure 1.13 shows a magnification of the quasi-plastically deformed subsurface of a glass-ceramic composite from a central section region where the microfailures at weak interfaces between mica platelets and glass phase may be observed. Here, the damage has become so intense (due to high loading or large numbers of cycles) that neighboring microcracks coalesce. Further damaging may lead to extensive material removal or to complete breakdown

of the material, due to formation of macroscopic cracks that grow in a radial direction. As a result, materials in which this occurs tend to be more susceptible to wear.

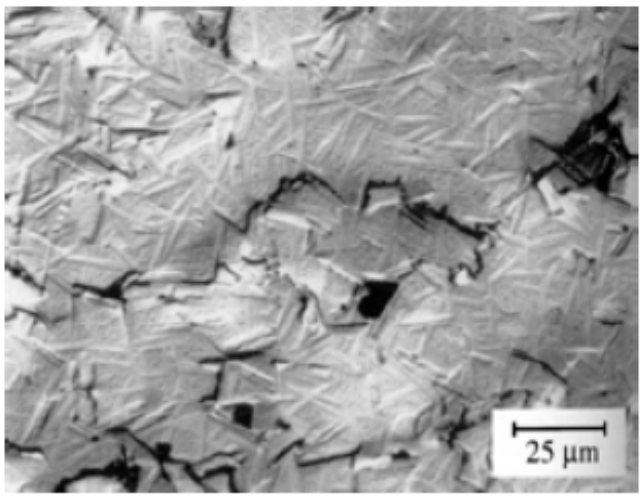

Figure 1.13. Micrograph of the subsurface of a glass-ceramic that shows microcracks at weak interfaces between mica platelets and the glass phase coalescing. [2]

The shear-faults are finely and discretely distributed in the quasi-plastic zone, as shown in Figure 1.14(a). These faults are impeded from growing as the compressive stresses work such to close the sliding shear-fault. As a consequence, the only way for them to relax further increasing tension is to generate microcracks (or wingcracks) at the tip of the defects (Figure 1.14(b)).

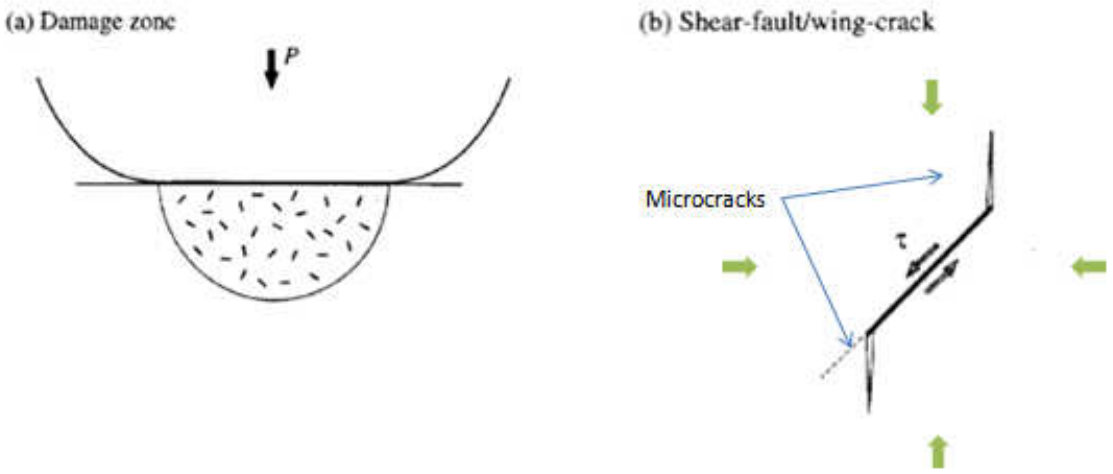

Figure 1.14. Illustration of shear-fault/wing-cracks system: (a) array of shear faults forms under contact load *P* in the quasi-plastic zone, (b) individual shear-fault with wing-cracks. [1]

The contact-induced quasi-plasticity is manifested above a threshold yield load, P_Y, defined combining equations (8) and (11), giving

$$P_Y = \frac{9}{16}\frac{(1.1\pi Y)^3}{E^{*2}}r^2 \tag{15}$$

This expression can be written as a function of the material's hardness, H, considering that $H = eY$, where e is a dimensionless constant (for metals e=3). This leads to the final expression for the quasi-plastic yield load being:

$$P_Y = QH\left(\frac{H}{E^*}\right)^2 r^2 \tag{16}$$

where Q is a dimensionless constant.

1.2.3 Strength degradation from contact damage

Once damage is induced within the material, it is of great interest to study the consequences of it, particularly from the perspective of assessing how damage tolerant the material is. This is done by evaluating the corresponding residual mechanical strength, either by four-point, three-point or biaxial flexure tests. The information obtained from these tests gives a quantitative measure of the damage introduced by contact loading, and explain the real effect of it on mechanical strength. Such knowledge is crucial in many structural and wear applications involving brittle materials such as ceramics and cemented carbides.

The residual strength of previously indented specimens under single-punch loading (contact load is applied during a certain time and then released) has already been carried out for a variety of ceramics and also for some cemented carbides. In all these studies a significant microstructure dependency is clear. With increased loading, the radius of the contact impression expands and from a critical value on, the hereby introduced damage is dominant such that specimen failure occurs at the indentation site. Figure 1.15 show surface details of three silicon nitrides with fine (F), medium (M), and coarse (C) microstructures, where it is observed that the failure originates from the bases of cone cracks in the F and M grade, whereas it in the C grade originates in subsurface damage zones [1].

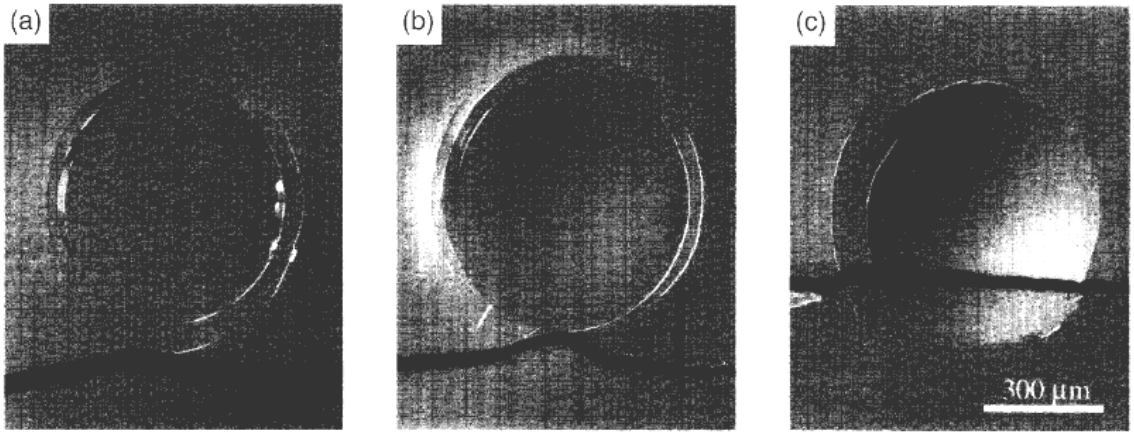

Figure 1.15. Contact failure sites in silicon nitride specimens of (a) fine, (b) medium, and (c) coarse microstructure. [1]

In Figure 1.16, the strength of the same silicon nitrides are plotted as a function of previously applied indentation load.

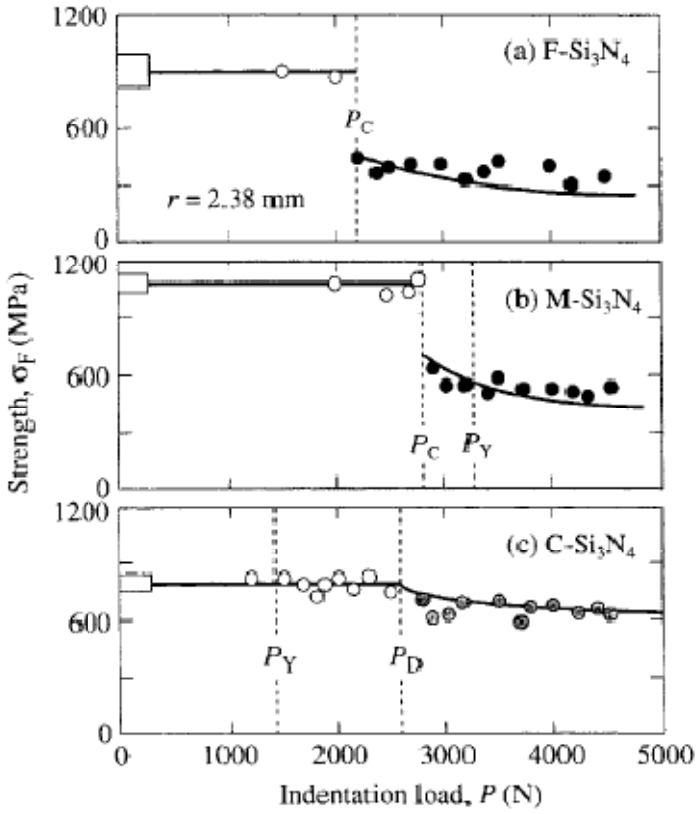

Figure 1.16. Fracture strength as a function of indentation load for (a) fine-, (b) medium-, and (c) coarse grade silicon nitride. Experimental measurements are represented by black, gray and open points. Black symbols indicate failure origin in cone cracks, gray symbols in quasi-plastic zones, and open symbols in other (intrinsic) defects. Solid curves are theoretical fits. Original strength values of polished, unindented specimens are represented by boxes at left. Vertical dashed lines represent critical loads. [1]

In the fine- and medium grained grades, an abrupt drop in strength is observed at the critical load for cone crack initiation, and thereafter the strength decreases gradually. For the coarse grade, on the other hand, the mechanical strength decreases only slightly and this takes place after some buildup of damage intensity, above $P_D \approx 2P_Y$. The different behaviors indicate that materials with coarser microstructure are more damage tolerant, although at higher loads or under fatigue loading the coalescence of microcracks may generate highly accelerated strength losses.

Similar behavior was observed for relatively brittle cemented carbides, as shown in Figure 1.17. Here, I and K refer to ultrafine grades where C corresponds to a rather fine one. In all three cases a sudden drop in strength is demonstrated at a contact load defined as critical, the relative strength loss being more significant for in the C grade.

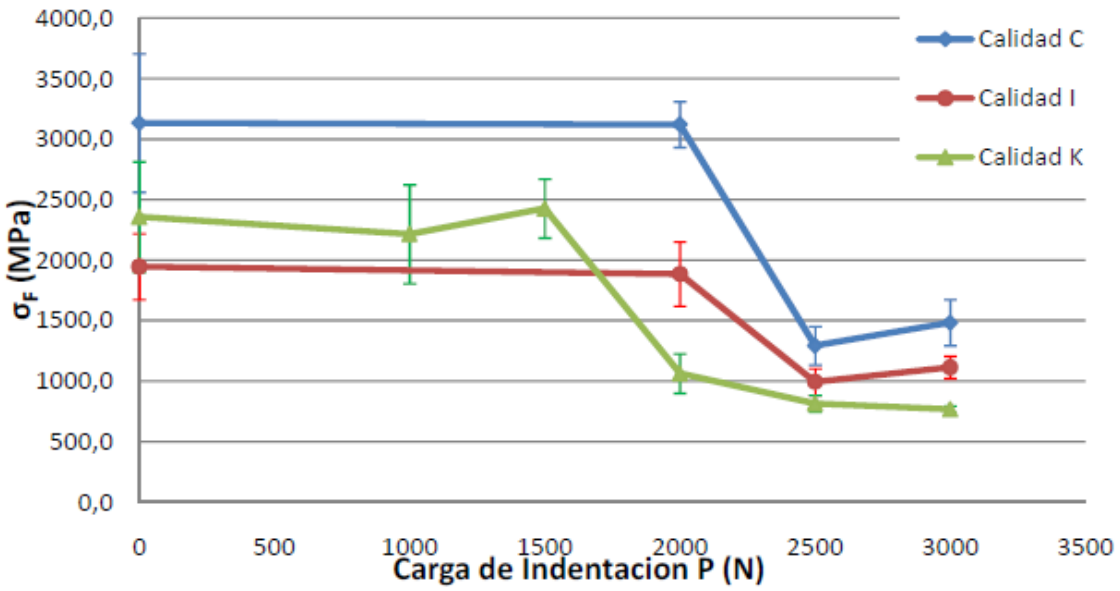

Figure 1.17. Residual fracture strength for three grades of cemented carbide indented with tungsten carbide pin (r = 2mm). Data points represent mean values of the experimentally measured strength. [5]

The effect on the strength for specimens subjected to fatigue loading has not yet been investigated for cemented carbides, and in consequence this final year project aims to explore this field. However, studies have been brought out on several ceramic materials focusing also in this case on the role played by the microstructure. Figure 1.18 shows the results of two studies made on silicon carbide (a) and on the same silicon nitrides as mentioned above (b).

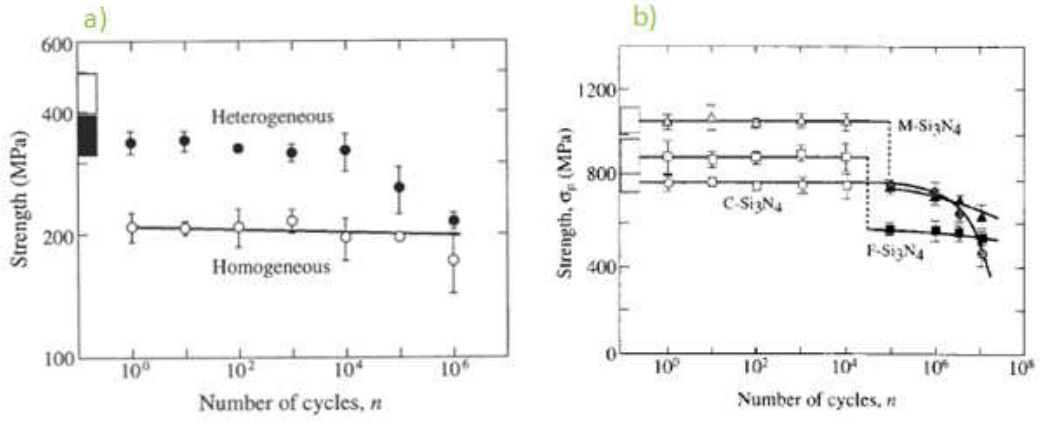

Figure 1.18. (a) Fracture strength as a function of indentation fatigue cycles for homogeneous (open symbols) and heterogeneous (black symbols) silicon carbide (tungsten carbide sphere of radius 3.18mm and *P* =1000 N at frequency 10 Hz). Data points represent mean values and the curve is predicted strength degradation from slow crack growth for the homogeneous material. Boxes at left indicate values of unindented specimens. [6] (b) Fracture strength for silicon nitrite specimens subjected to fatigue (tungsten carbide sphere of radius 1.98 mm and *P* =1000 N at frequency 10 Hz). Data points represent experimental measurements; closed symbols represent failures from cone cracks or quasi-plastic zones, open symbols from other origins. Boxes at left represent strengths of polished, unindented specimens.[1]

Figure 1.18(a) demonstrates that the homogeneous silicon carbide suffers an important decrease in mechanical strength upon contact, result of the formation of a cone crack. However, this strength degradation as a function of number of cycles is rather slight due to the slow crack growth. On the other hand, the heterogeneous silicon carbide maintains strength intact up to 10^4 cycles, but then experiences a significant degradation caused by coalescence of microcracks [6].

In Figure 1.18(b), the F and M silicon nitride grades suffer an abrupt loss of strength at a certain number of cycles, followed by a slow increasing degradation for higher number of cycles. As for the silicon carbide case, the coarse grade maintains the mechanical strength almost up to one million cycles, before decreasing rapidly due to the coalescence of microcracks [1].

Following the ideas mentioned above, this final year research project aims to broaden the knowledge of the mechanical behavior of brittle and relatively ductile cemented carbides subjected to monotonic and cyclic contact loading. The precise objectives set up and the methods used will be presented in the following sections.

2. Objectives of the study

The global objective of this project is to study the damage that can be introduced into cemented carbides by spherical indentation and its influence on the resulting residual mechanical strength of the material. The study is carried out in two different grades of cemented carbides such to evaluate the influence of microstructure on the mechanical behavior of these. In order to fulfill this objective, the following activities are defined as relevant:

- Mechanical characterization of the different hardmetal grades, in terms of Vickers hardness, fracture toughness and the modulus of elasticity.

- Introduction of Hertzian contact damage in the distinct cemented carbide grades, under monotonic and cyclic loading conditions.

- Assessment of the damage evolution as a function of contact load and microstructure of the material.

- Evaluation of residual (four-point bending) strength in the cemented carbides, resulting from the introduced contact damage.

- Correlation of damage effects on the material properties as related to microstructural parameters for the different hardmetal grades.

The methods used to successfully achieve these steps will be described in the following section.

3. Materials and methods

3.1 Materials

3.1.1 Cemented carbides

The materials studied in this project are supplied by Sandvik Hard Materials. Two different grades of cemented carbides, referred to in this investigation as E and C, are studied. Their microstructural compositions are shown in Table 3.1. Both grades may be considered as composites with heterogeneous microstructures, although clearly C is expected to be harder and less tough than E, due to the finer grain size and lesser binder content of the former.

Table 3.1. Microstructural parameters; binder content and carbide grain size, for the two hardmetal grades C and E, studied in this project.

Hardmetal grade	Binder content (%wt Co)	WC grain size (µm)
C	10	0.4
E	22	0.9

3.1.2 Preparation of specimens

The two hardmetal grades were received as rectangular beams with cross section dimensions 45 x 3,6 x 3 mm. In order to eliminate any potential surface flaws related to the fabrication process all the specimens were ground and polished in several steps until a perfectly mirror-like surface finish was attained. In addition, the surface edges were chamfered such to eliminate potential stress risers. For this, manual polishing systems STRUERS LaboPol-5 and Buehler Alpha were used. Grinding was conducted by using magnetic diamond-containing discs (STRUERS MD-Piano) of increasingly finer particle size: 120, 220, 600, and 1200, using water as lubricant. Subsequent polishing was carried out by using a softer disc (STRUERS MD-Dac) and a diamond containing liquid suspension with grain sizes of 6 µm (first) and 3 µm (second) together with a Kemet lubricant fluid type GW2. Final polishing was attained using the STRUERS MD-Nap disc, adding a Buehler non-crystallizing colloidal silica polishing suspension with a grain size of 0.5 µm in combination with the same lubricant.

Forces applied during polishing of the specimens were always low, attempting to eliminate any residual surface stresses that could be induced by earlier grinding steps. As a result, a mirror-like surface-finish free of residual stresses was finally obtained (Figure 3.1).

Figure 3.1. Polished C grade specimens.

3.2 Mechanical characterization

The mechanical characterization of the C and E hardmetal grades was carried out by means of evaluating Vickers hardness and fracture toughness, as well as the modulus of elasticity.

3.2.1 Vickers hardness and fracture toughness

The hardness of a material is defined as its resistance to localized plastic deformation and can be measured by the Vickers test technique, i.e. by using small diamond indenters with pyramidal geometry. These are applied into the material with a certain force, such that the surface of the specimen is left with a deformation imprint like the one seen in figure 3.2. This deformation is later observed and measured under a microscope, and finally converted into a hardness number.

Surface polished samples of the two hardmetal grades under consideration were subjected to a Vickers load of 30 kg, using a FRANK durometer of type 532, during 20 seconds. The imprints generated by this load were then observed with the optical microscope OLYMPUS LEXT model OLS 3100. Five indentations were made in each specimen.

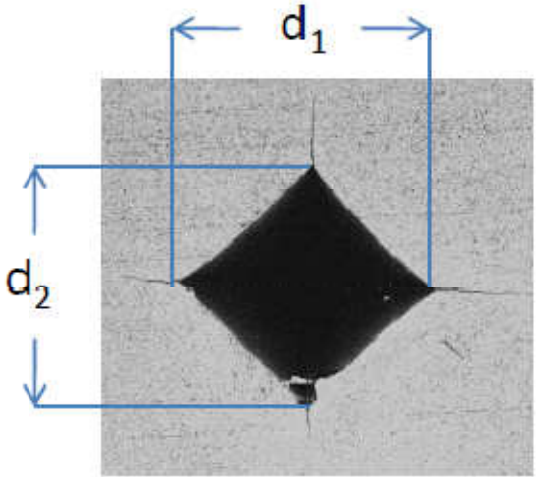

Figure 3.2. Vickers imprint on the hardmetal grade C, generated by a load of 30 kg.

The hardness number is calculated taking measurements of the two diagonals of the imprint left by the indenter as demonstrated in Figure 3.2, and the applied indentation load according to:

$$H_v = \frac{1{,}854P}{d^2} \tag{17}$$

where P is the indentation load in Newtons and d is the mean value of the two diagonals of the imprint in meters (from Figure 3.2: $d = \frac{d_1+d_2}{2}$).

This same technique can be used to estimate the fracture toughness of a material. The fracture toughness defines the resistance of a material to crack propagation and hence, its capacity to absorb energy before breaking. For the evaluation of this, the cracks extending from the corners of the Vickers imprint (known as Palmqvist cracks) are measured and used in the following expression:

$$K_{IC} = \frac{\alpha P}{d l^{1/2}} \tag{18}$$

where α is an empirical, semi empirical or theoretical coefficient with the value 0.03026, d is the length of the half-diagonal of the indentation imprint, and l the mean value of the superficial Palmqvist cracks.

This is a simple and rapid method to calculate a fracture toughness value, although for it to be valid, the Palmqvist cracks need to be longer than the half-diagonals of the Vickers impression.

3.2.2 Modulus of elasticity

The modulus of elasticity, also called Young's modulus, defines the stiffness of a material, i.e. its resistance to elastic deformation. Stiffer materials posses a superior modulus, meaning that smaller elastic strain will be generated as a result of the application of a given stress.

A simple, nondestructive method of determining the modulus of elasticity is based on the standard ASTM E-1876 [7]. In short, it consists in measuring the natural vibration frequency of the material from its response to a light mechanic impulse.

The test is carried out placing the specimen on supporting "cushions" in order to isolate it of vibrations from the surroundings. The acoustic sensor Grindosonic is then put in contact with one of the lateral surfaces of the specimen and a light hit is applied at the center of the specimen surface. The sensor displays automatically the value of the natural vibration frequency, f_f, with a precision of 5 significant digits. Together with the dimensions of the specimen, Young's modulus can finally be calculated as follows:

$$E = 0.9465\left(\frac{m{f_f}^2}{b}\right)\left(\frac{L^3}{t^3}\right)T_1 \tag{19}$$

where m is the mass (g), b the width, L the length and t the thickness of the specimen (mm). T_1 is a factor that takes into account the finite dimensions of the specimen and can be expressed as

$$T_1 = 1 + 6{,}585(1 + 0{,}0752\nu + 0{,}8109\nu^2)\left(\frac{t}{L}\right)^2 - 0{,}868\left(\frac{t}{L}\right)^4\left[\frac{8{,}340(1 + 0{,}2023\nu + 2{,}173\nu^2)\left(\frac{t}{L}\right)^4}{1{,}000 + 6{,}338(1 + 0{,}1408\nu + 1{,}536\nu^2)\left(\frac{t}{L}\right)^2}\right] \tag{20}$$

where ν is Poisson's ratio.

3.3 Spherical indentation

The Hertzian contact tests were carried out using an INSTRON model 8511 with a hardmetal pin (10%wt cobalt and carbide grain size about 0.4µm) of radius 1.5mm (Figure 3.4).

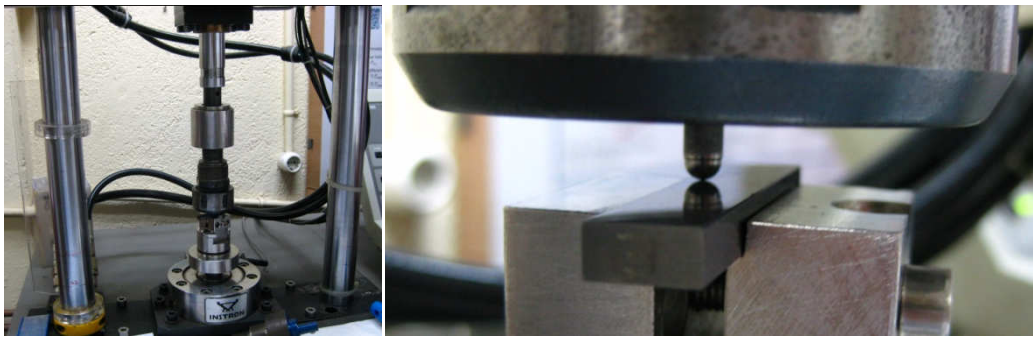

Figure 3.4. Servo hydraulic machine INSTRON of model 8511 (left) and tungsten carbide pin GD13 with radius of curvature =1.5mm applying contact load on a grade E specimen (right).

The first series of measurements were taken under monotonic loading, where loads were applied to the specimens at a speed of 30 N/s, held for 20 seconds and removed at a speed of 50 N/s (see figure 3.5 (a)). Cyclic loading was applied with a sinusoidal wave form taking $R = \frac{\sigma_{min}}{\sigma_{max}} = \frac{P_{min}}{P_{max}} = 0.1$ (Figure 3.5(b)). Applied frequency varied with the numbers of cycles, with a maximum of 20 Hz for tests corresponding to elevated numbers of cycles.

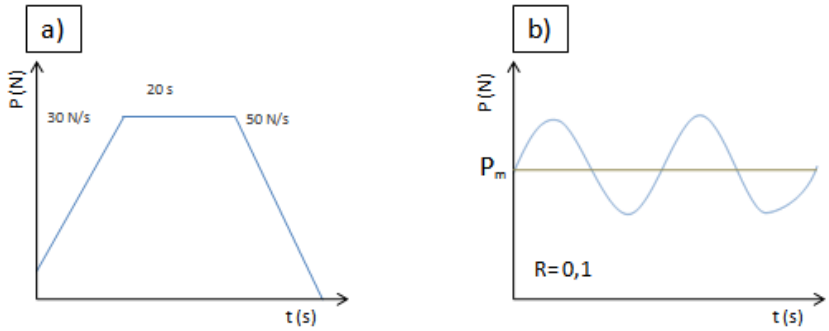

Figure 3.4. Applied loading cycles for (a) monotonic and (b) cyclic indentation tests.

For the evaluation of surface damage, one specimen of each grade was used and the indentations were positioned with about 5 mm of space in between each. Residual mechanical strength was assessed on specimens containing three indentations each. These were placed one in the middle and the others placed with 5mm spacing to each side of the center

indentation. Exceptions were made for the specimens subjected to 10^4 and 10^6cycles, on which two and one indentations were made, respectively.

Table 3.2 presents a chart of the contact loads and numbers of cycles applied to each specimen for the different test series.

Table 3.2. Experimental scheme with the corresponding spherical indentations employed.

Indentation series	**Cemented carbide grade**	**Contact loads (N)**	**Number of cycles, n**
Surface damage evolution.	E	500, 1000, 1500, 2000, 2500, 3000, 3500, 4000	1
	C	500, 1000, 1500, 2000, 2500, 2600, 3000, 3500	1
	E and C	2000 , 2500	1, 10, 10^2, 10^3, 10^4, 10^5
Evaluation of strength degradation associated with damage induced under monotonic loading.	E	300, 500, 1000, 1500, 2000, 2500	1
	C	1500, 1750, 2000	1
Evaluation of strength degradation associated with damage induced under cyclic loading.	E	500, 2000	1, 10^2, 10^4, 10^6
	C	2000	1, 10^2, 10^4, 10^6
Subsurface analysis of damage introduced under monotonic loading.	E and C	1750, 2000, 2500, 3000	1
Subsurface analysis of damage introduced under cyclic loading.	E and C	2000	10^2, 10^4, 10^6

Indentation loads for fatigue tests were chosen depending on the materials' response to monotonic contact. For hardmetal grade C, it was based on the findings of recent studies from the research group where this investigation is conducted [5, 10]. These investigations revealed that for grade C specimens previously indented with P =2000N, fracture in four-point bending was sometimes observed in direct relation to the indentation site, i.e. failure origin correspond

to introduced damage, although without any strength degradation. A similar critical load for which this behavior could be observed in hardmetal grade E was then also attempted here. Additionally, both materials were subjected to fatigue loading with P_{max} =2000N for comparative reasons. Finally, the response of grade E specimens to fatigue contact at its critical load was evaluated too.

After indentation, surface specimens were observed using the optical microscope. Image analyzer was used to measure the contact radius, *a*, for each indentation such to obtain the indentation stress-strain curve. Images were saved to be used for the study of damage evolution.

In order to observe the damage generated in the subsurface section of the materials, split-and-bond specimens were prepared. Preparation consisted in sectioning given specimens in half-blocks, grind and polish the corresponding cross-section, and finally bind them back with a thin adhesive layer (not exceeding a thickness of 10 μm). The new top surface, perpendicular to the polished interfaces, was then polished again and indentations were made along the bonding line (Figure 3.6). Prior to indentation, bonded specimens were mounted on Bakelite, which provided an outer support of the same. After indentation, the adhesive was dissolved in acetone under ultrasonic vibrations.

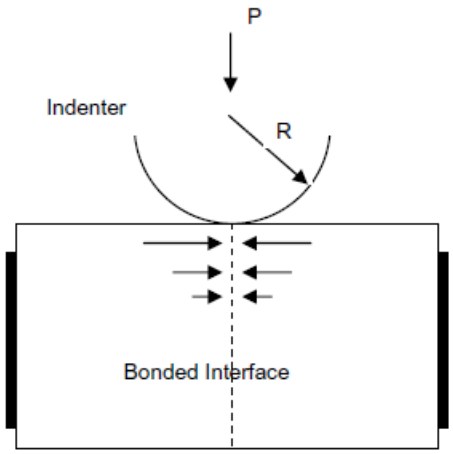

Figure 3.6. Split-and-bond specimen as subjected to Hertzian indentation. [3]

3.4 Fracture strength

Based on the brittle-like nature of cemented carbides, for evaluating their fracture strength flexural test are preferred over standard tensile tests. Hence, specimens were flexural tested using a four-point loading configuration until fracture occurred. The specimens were placed with the indented surface turned to the bottom as this is the side experiencing tensile stresses during bending.

The fracture stress of the material is calculated from the specimen dimensions, the bending moment and the moment of inertia of the cross section. By introducing the applied load at which fracture was observed, flexural strength and was determined from

$$\sigma_{fs} = \frac{3P_f L}{2\omega d^2} \tag{21}$$

where P_f is the load at fracture (N), L is the distance between support points (m), and ω and d correspond to the width and depth of the specimen (m).

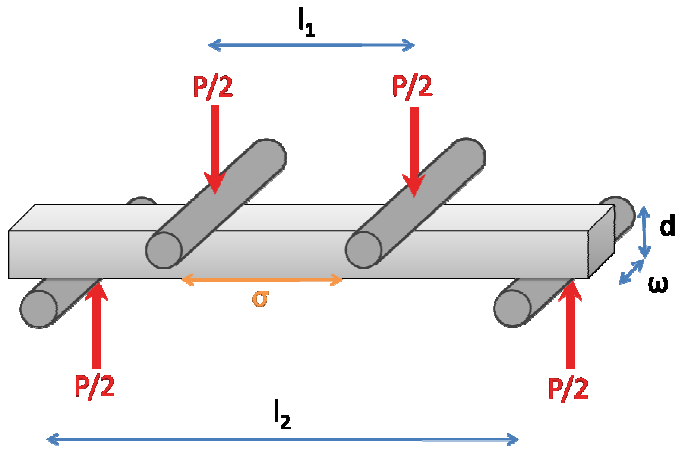

Figure 3.6. Test configuration of the four-point flexural tests.

Figure 3.6 shows an illustration of the flexural test configuration, where $L=l_2-l_1$. This distance was of 20 mm (with l_2 = 40mm and l_1 = 20mm). Tests were carried out in ambient temperature and humidity, using a servo hydraulic machine INSTRON (model 8562). Load was applied at a speed of 50 N/s. At least three specimens were evaluated for each hard metal grade and indentation load level.

Finally, fractured specimens were observed by means of scanning electron microscopy (Figure 3.7), and failure sites identified.

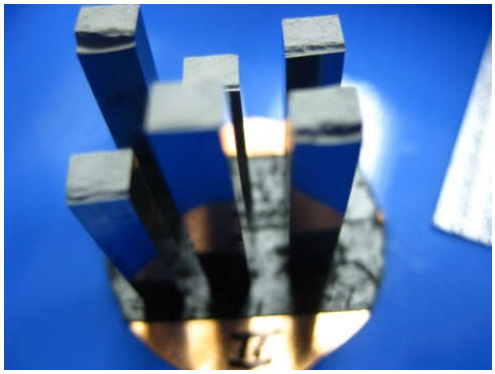

Figure 3.7. E grade specimens as prepared for fractographic analysis with SEM.

4. Results and discussion

4.1 Mechanical characterization

Micrographs of the Vickers indentations generated in hardmetal grades C and E, for an applied load of 294N are shown in Figure 4.1. It is clear there that the Vickers imprint left in grade C is smaller than that in grade E. This indicates that the former is more resistant to irreversible deformation and hence possess a superior hardness than the latter. It is also observed that in addition to a greater imprint, grade E lack completely of any type of Palmqvist cracks. As a result, the fracture toughness of this material may be estimated as tougher than for grade C, but calculation of an absolute value is not possible through this technique. In these cases, the use of real precracked specimens is needed but then testing gets more complex.

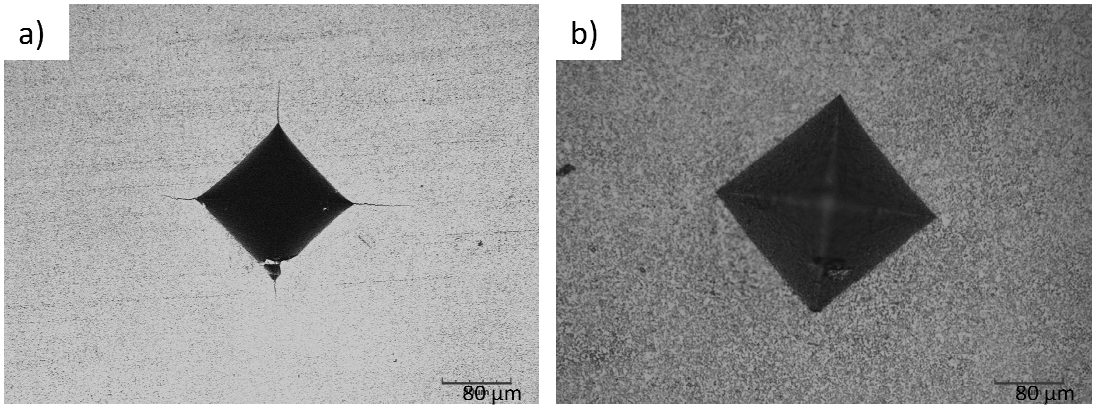

Figure 4.1. Vickers indentation impressions generated by application of Vickers load of 30 kg in cemented carbide grades (a) C and (b) E.

Table 4.1 presents the results obtained by applying the methods mentioned in the former part to calculate Vickers hardness, fracture toughness, and modulus of elasticity of grades C and E. Toughness values calculated using mentioned precracked specimens are also displayed in Table 4.1.

As indicated by observations of the micrographs, cemented carbide grade C presents a superior hardness value than grade E. In turn, grade E demonstrates a mechanically tougher behavior as it proves to be able to irreversibly deform in absence of crack generation. In terms of Young's modulus, grade C is found to be stiffer than grade E.

Table 4.1. Mechanical properties of the cemented carbide C and E grades.

Properties	Grade C		Grade E	
Vickers hardness (GPa)	**15.3**		**7.71**	
Vickers fracture toughness ($MPa.m^{1/2}$)	**13.4**	**10.4±0.3[1]**	**--**	**15.2±0.3[1]**
Modulus of elasticity (GPa)	**586**		**442**	

These results may be completely rationalized on the basis of microstructural differences between the materials studied. A lesser content of metallic binder (as for the C grade) suggests greater hardness and stiffness, and are thus in accordance with predictions made in the literature [8]. It is also worth mentioning that the smaller carbide grain size of grade C is a contributing factor to the greater hardness of the same [8].

4.2 Spherical indentation

Figures 4.2 and 4.3 display the evolution of introduced damage in grade C and E specimens respectively, generated by contact loads applied monotonically, ranging from 1000 N to 3500 N.

Both hardmetal grades present sink-in imprints, product of the materials´ quasi-plasticity, that increase in size with rising load. This imprint is for all load levels greater in size for grade E specimens. Hence, superior applied load values are needed to generate a contact impression of the same size in grade C materials, as demonstrated by the graph in Figure 4.4. This observation reflects the resistance to irreversible deformation, being hence superior in hardmetal grade C.

For the harder grade, contact loads exceeding 2000 N are found to induce initiation and propagation of annular cracks, which multiply when the material is subjected to even higher loads. The load ranges critical for different cracking events are in complete agreement with

[1] Fracture toughness measured using a crack propagation technique; SENB

those previously identified by Góez and coworkers [10], predicting nucleation and growth up to ¼ circular crack to occur at load levels of 2000-2500N, singular circular crack for load levels ranging from 2500-3500N, and multiple circular cracks above 3500N. In accordance, the crack evolution observed in this study showed crack initiation for indentation load levels of about 2600 N, a full circular crack distinguished at 3000N and presence of multiple cracks at 3500N. However, in this regard it is interesting to note that the E grade does not exhibit any cracking phenomenon within the range of applied load studied.

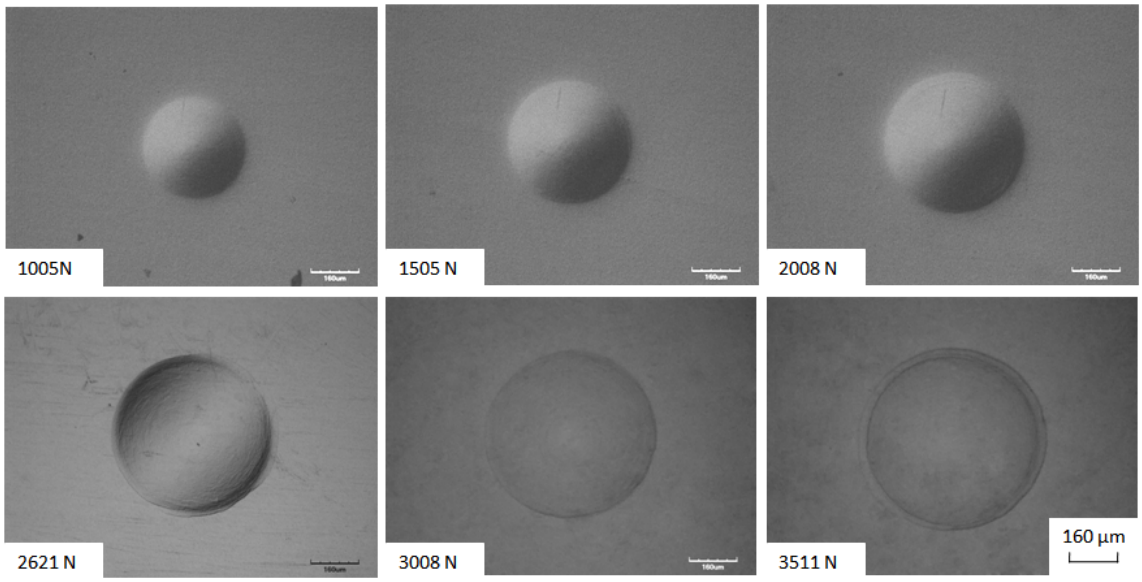

Figure 4.2. Surface damage evolution in cemented carbide grade C under increased monotonic contact loading.

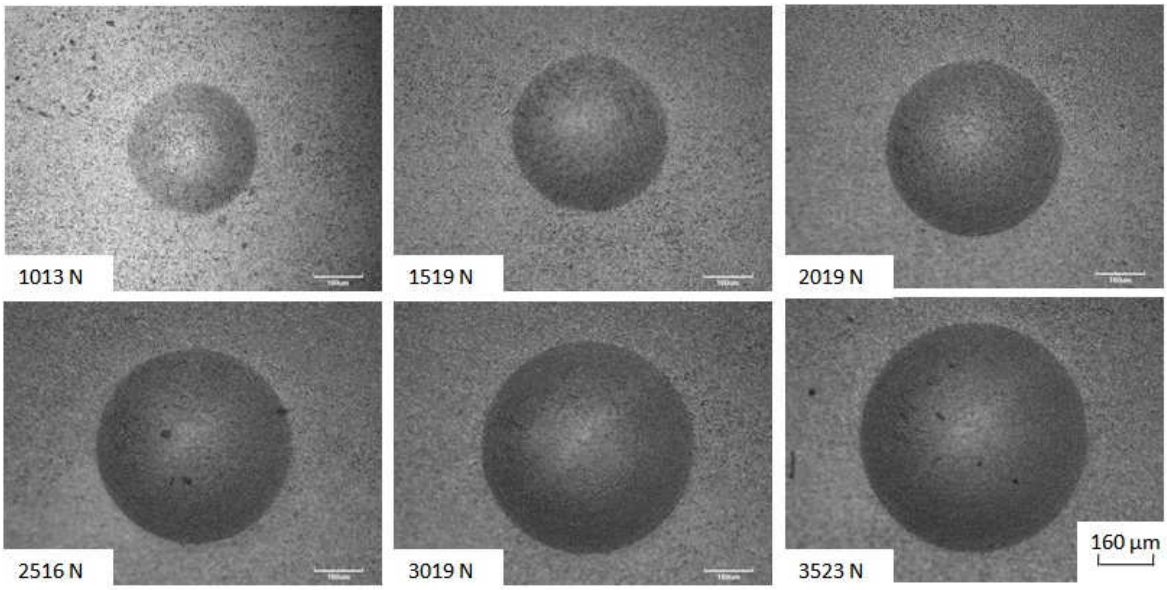

Figure 4.3. Surface damage evolution in cemented carbide grade E under increased monotonic contact loading.

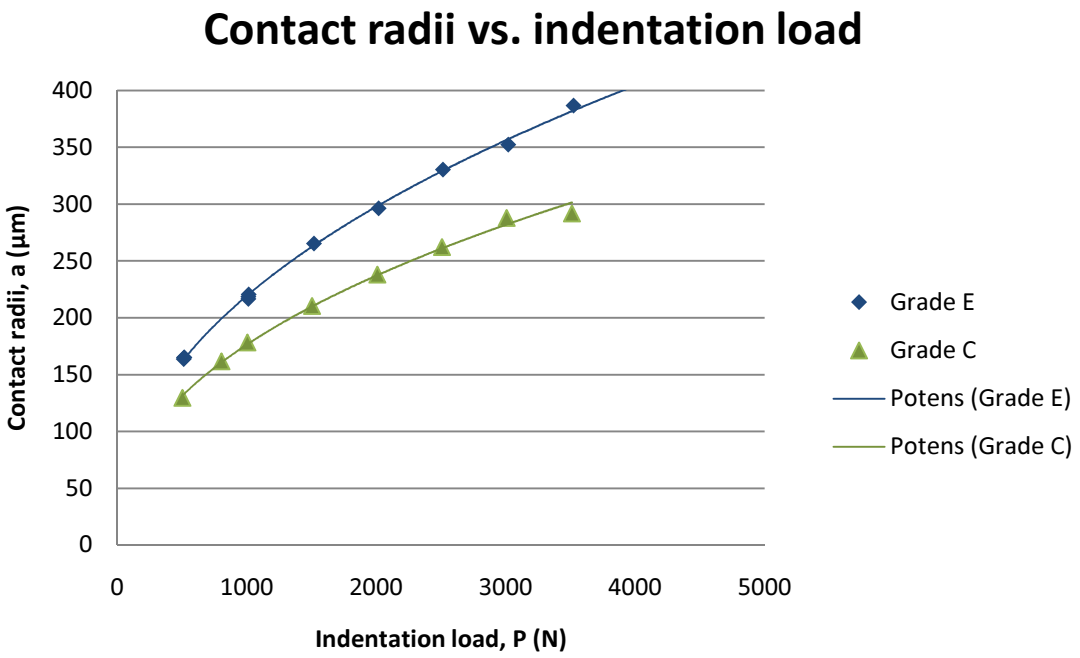

Figure 4.4. Contact radii as a function of indentation load for hardmetal grades E and C.

Taking into consideration the pin radius, *r*, the measured contact radius for each load, *a*, and the applied load, *P*, an indentation stress-strain curve can be constructed, taking stress as $p_0 = \frac{P}{\pi a^2}$, and defining strain as $\frac{a}{r}$. Curves for the two hardmetal grades are displayed in Figure 4.5, where data points are experimental values, dashed lines correspond to the calculated Hertzian elastic response (from Equation (4)), and full drawn lines are curves fitted to data points.

To a beginning, the indentation stress increases linearly with strain as predicted by the Hertzian relation, indicating an elastic response to contact. Further, a yielding behavior is observed as the curves deviate from linearity. Above this point, the indentation stress increases monotonically with indentation strain until reaching high strain values, where the stress levels off.

It is demonstrated that yielding occurs at an inferior indentation stress in hardmetal grade E than in grade C, which again reflects this material's higher susceptibility to irreversible deformation. The following monotonic increase in stress corresponds to the yielding of cobalt binder phase [3]. With this in mind, the extensive strain behavior of grade E may be subscribed to its binder content, which is almost twice the value of that of grade C.

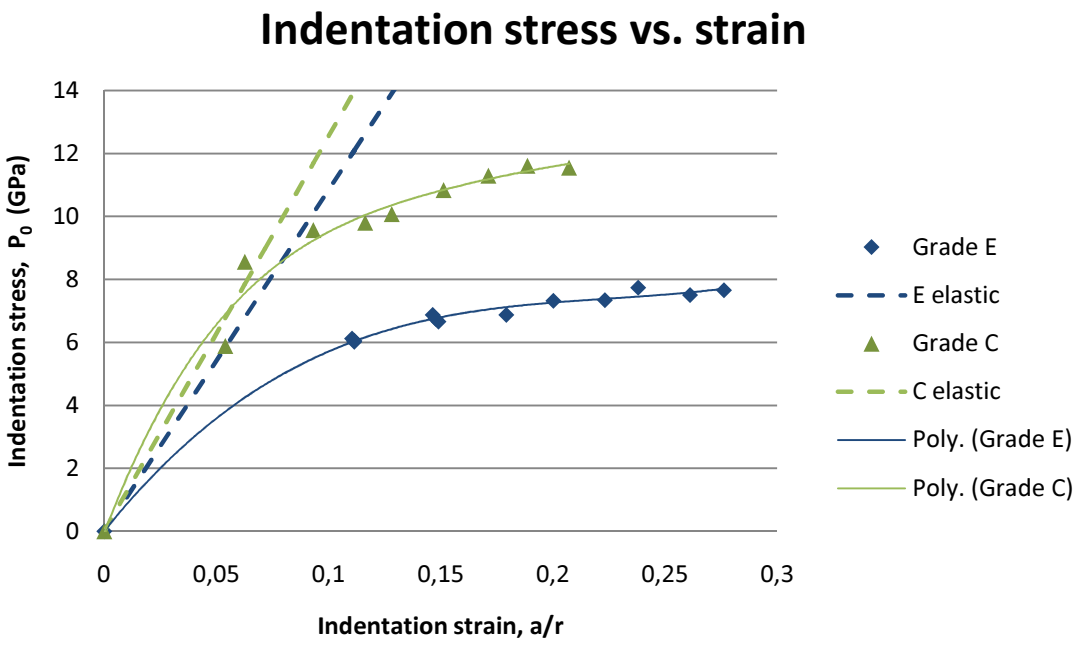

Figure 4.5. Hertzian indentation stress-strain curves for hardmetal grades E and C. The dashed lines correspond to the calculated Hertzian elastic response.

The final stage of the indentation stress-strain curve represents plastic deformation of both phases, i.e. including deformation of the tungsten carbides [12]. This deformation can be observed due to the relatively coarse microstructure of hardmetal grade E, for which a detailed study of the microstructural response to contact loading was conducted using the scanning electron microscope. Observations at relatively high magnification indicate presence of various microfractures in the quasi-plastically deformed zone beneath the contact area, as well as slip lines within tungsten carbides situated in the same zone.

Figure 4.6(a)-(b) shows and compares the microstructural aspect outside and within the deformed area, respectively, after monotonically applying a contact load of 3500N. The referred tungsten carbide slip deformation lines are quite clear in the micrograph to the right, whereas the fine lines visible over the whole area in both micrographs are simply polishing marks of the material. Cracks are also observed within the tungsten carbides located in the indentation subsurface area. These deformation mechanisms have been observed and recognized in earlier studies of hardmetals subjected to monotonic loading [3]. However, in the present study, the same observations are made in the zone beneath the indentation area of hardmetal grade E subsequent to cyclic loading (Figure 4.6(c)). Hence it is suggested that

quasi-plastic response to contact is analogous for high monotonic load levels, as well under high cycle fatigue at low load levels.

The finer and more homogeneous microstructure of hardmetal grade C makes a detailed study of its carbides difficult.

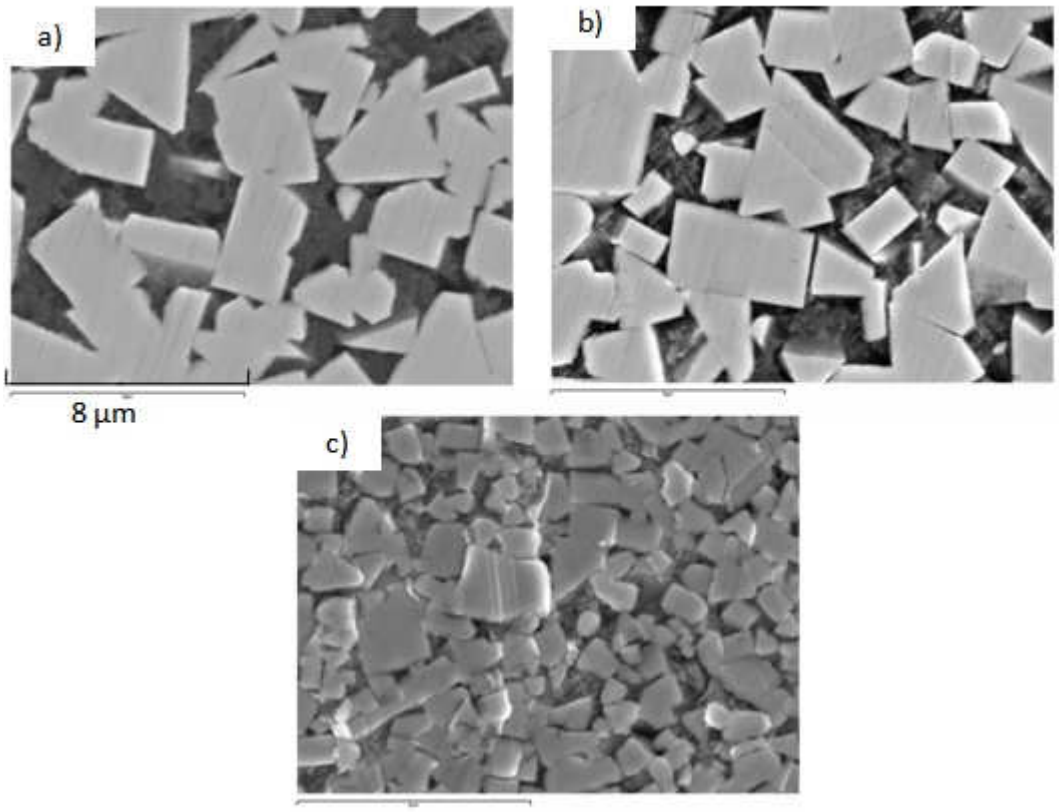

Figure 4.6. Enlarged views of the microstructure (a) outside and (b)-(c) within the quasi-plastically deformed area beneath the contact zone for hardmetal grade E, after being subjected to a monotonic contact load of P = 3500 N (b) and cyclic loading with P_{max} =2000N and n =10^6 cycles (c). Tungsten carbide pin used with radius 1.5mm.

Indentation stress-strain curves for grades C and E are presented in logarithmic form in Figure 4.7, where the dashed lines correspond to the elastic regime. Full drawn lines represent the plastic behavior of the materials and have been derived using as yield condition: $p_Y = \frac{1}{3}H_V$, where H_V is materials' hardness. The combination of these two curves allows following the complete mechanical behavior, from elastic to fully plastic, in terms of deformation of the materials, when subjected to Hertzian contact loading.

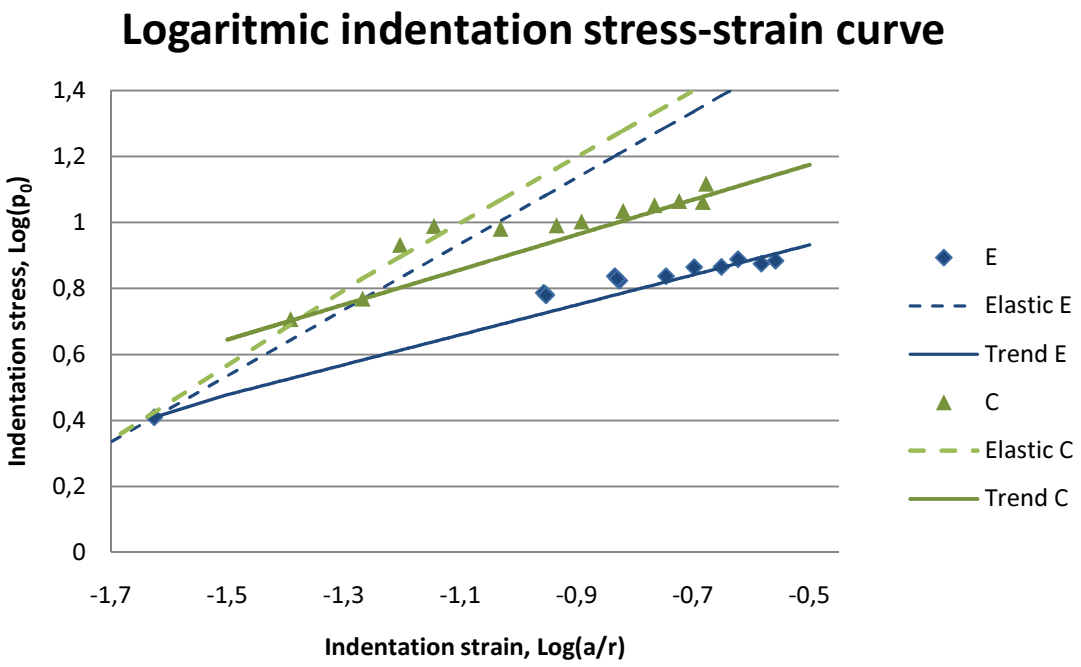

Figure 4.7. Logarithmic indentation stress-strain curve; data points are experimental values, full drawn lines are trendlines that allow the prediction of yielding behavior, and dashed lines correspond to the elastic response of the material established by Hertz.

Figures 4.8 and 4.9 show the evolution of surface damage for the C and E grades respectively, subjected to cyclic contact loads with P_{max} =2000 N and increasing number of cycles ranging from 1 to 10^5.

Similar to the behavior described under monotonic loading, E presents larger contact radius than grade C. However, in none of the two grades does indentation imprint vary in size as the number of cycles increases.

In grade C, appearance of annular cracks is noted after 10^3 cycles. It should be underlined that under monotonic loading, a value of 2000N was not enough for inducing any crack features in this grade. Moreover, a complete annular crack is observed after 10^4 cycles and at 10^5 cycles multiple ring cracks have been formed. The fact that this whole crack evolution takes place under cyclic loading at maximum applied load of 2000N, confirms the appropriateness of the contact load level chosen for these fatigue tests, in addition to the reasoning mentioned in section 3.2.3.

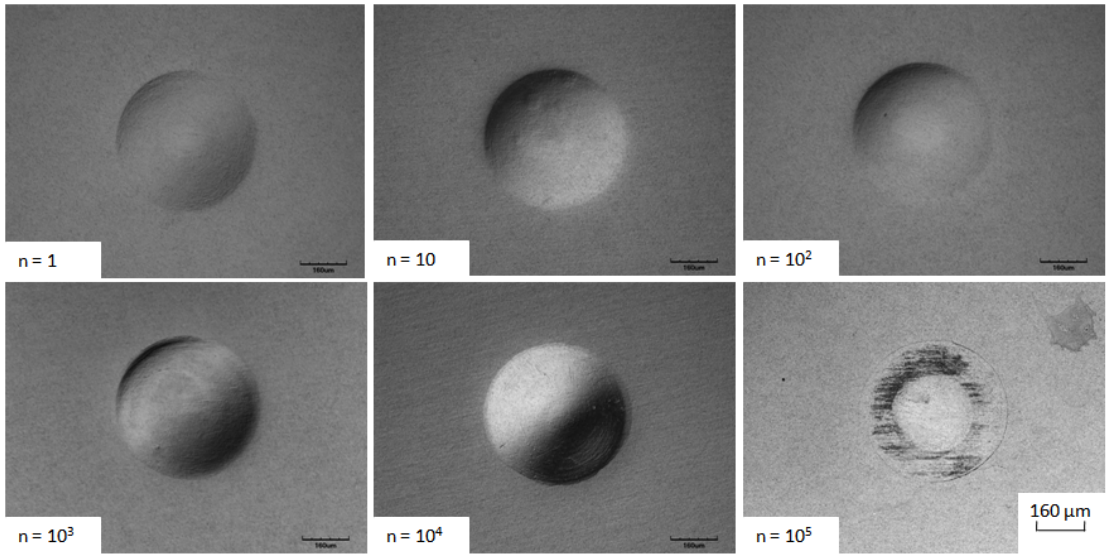

Figure 4.8. Surface damage evolution in cemented carbide grade C under fatigue contact loading with P_{max} =2000N.

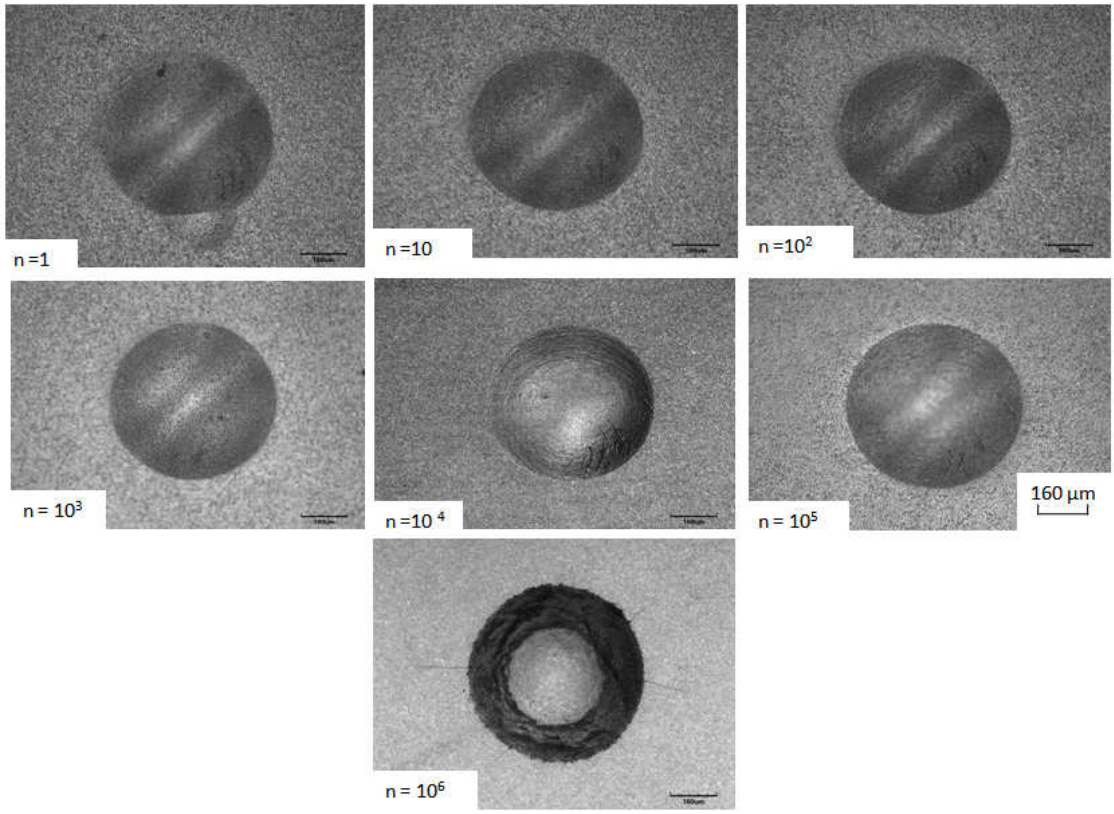

Figure 4.9. Surface damage evolution in cemented carbide grade E under fatigue contact loading with P_{max} =2000 N.

As it was already discerned under monotonic loading, hardmetal grade E does not exhibit any annular crack phenomenon during testing up to 10^5 cycles. However, a closer look into the indentation imprint contour allows to identify cracks of radial nature (Figure 4.10) which

appear after n =10^4 cycles. These radial cracks are clearly visible if number of cycles is increased up to 10^6 cycles.

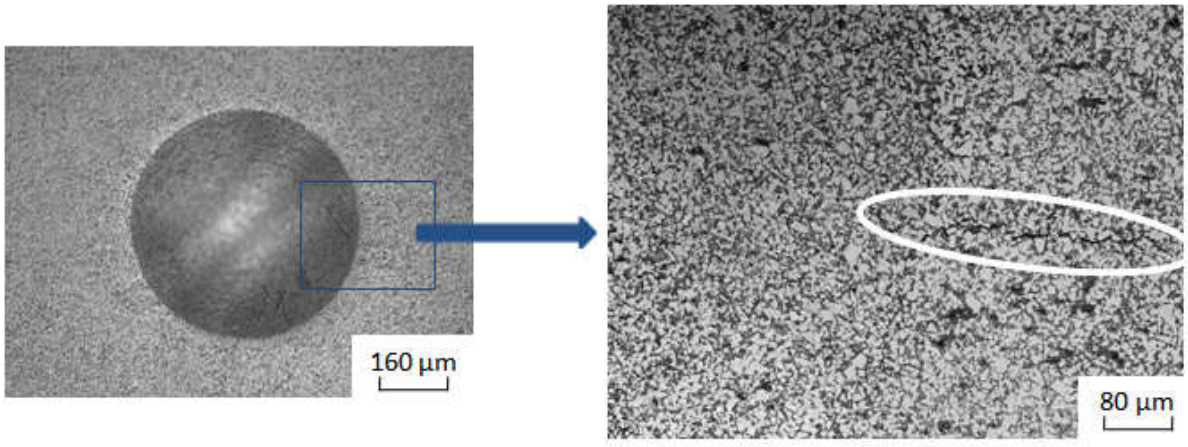

Figure 4.10. Magnification of the side section of contact imprint generated in cemented carbide grade E through fatigue loading with P_{max} =2000N and 10^5 cycles.

Nucleation of radial cracks occurs during the unloading cycle [3, 6, 13, 14] and takes place around the edge of the plastic zone, generated in the compressively stressed area beneath the contact circle upon indenting. Here, there is a transition from compressive to tensile stress, and once initiated in the compressively stressed area, the radial crack propagates rapidly through the tensile stress field up to the top surface, where it reaches its final crack size [3].

The subsurface damage evolution assessed on split-and-bond- specimens subjected to monotonic contact loads is revealed in Figure 4.11. For both materials, quasi-plastic deformation is observed. It expands gradually with increased loading. In grade E the quasi-plastic deformation is especially pronounced and no sign of brittle mode damage is found. In contrast, the C grade specimen shows presence of shallow cone cracks along with quasi-plastic damage already at P =1750 N.

Corresponding damage evolution, product of cyclic indentation tests with indentation load P_{max} =2000N is shown in Figure 4.12. Again, quasi-plastic deformation takes place in the two materials, the extension of which rises with the applied number of cycles. This damage is highly pronounced in grade E and it appears to take on an irregular shape at high cycling (i.e. comparing images at 10^4 and 10^6 cycles). Enlarged views enable to distinguish the presence of radial as well as shallow cone cracks at the indentation imprint contour, after application of 10^6 cycles. Figure 4.13 shows details of these.

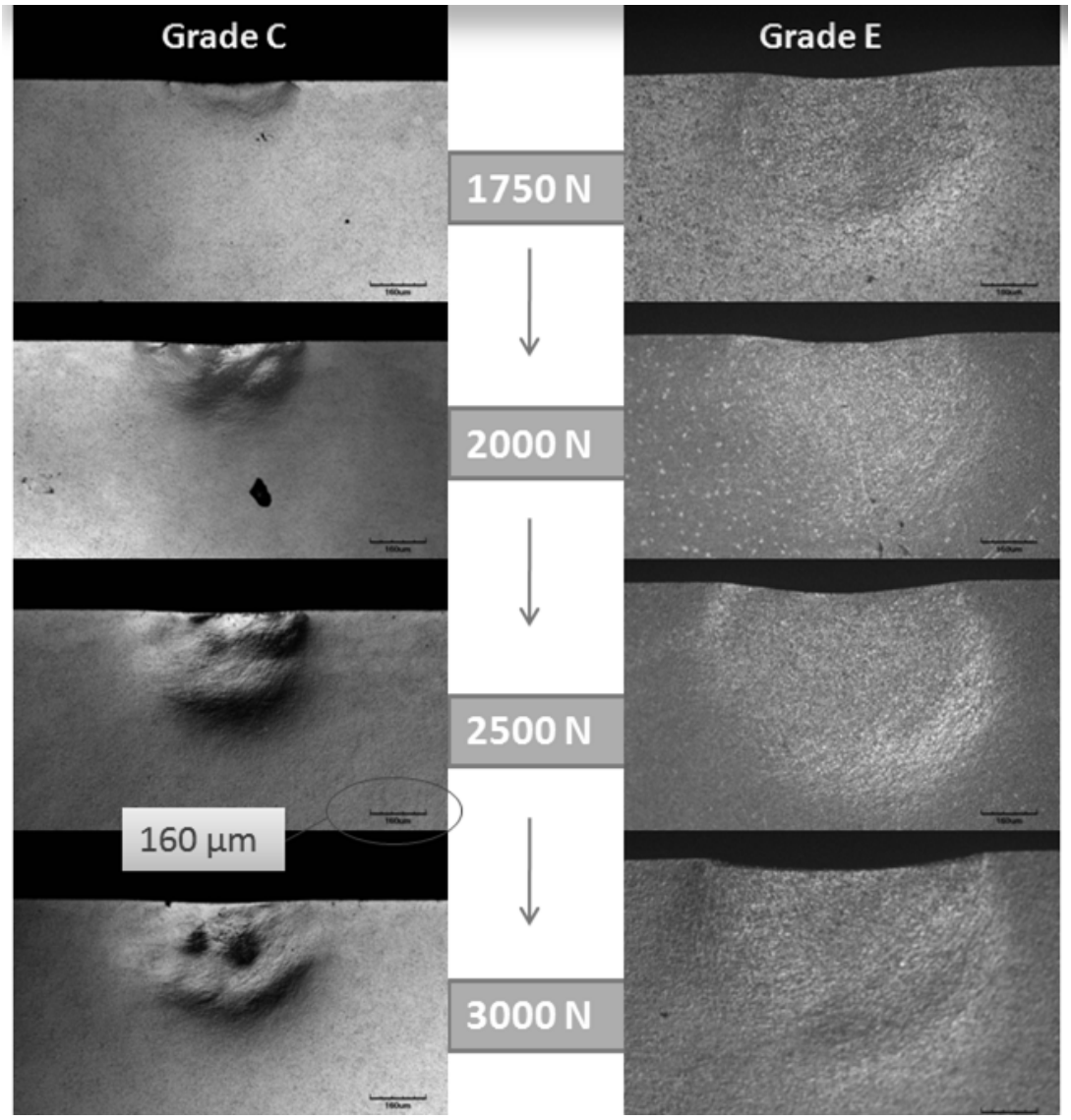

Figure 4.11. Subsurface damage evolution of cemented carbide grades C and E subjected to monotonic indentation loading with tungsten carbide pin of radius 1.5mm.

Hardmetal grade C also experiences mixed damage upon cycling. In this regard, quasi-plastic deformation, consistently smaller than in grade E, and cone cracking are both presented to a greater extent. Figure 4.13 shows corresponding surface and section views of indentation sites subjected to 10^4 and 10^6 cycles respectively, in which the two damage modes are clearly visible.

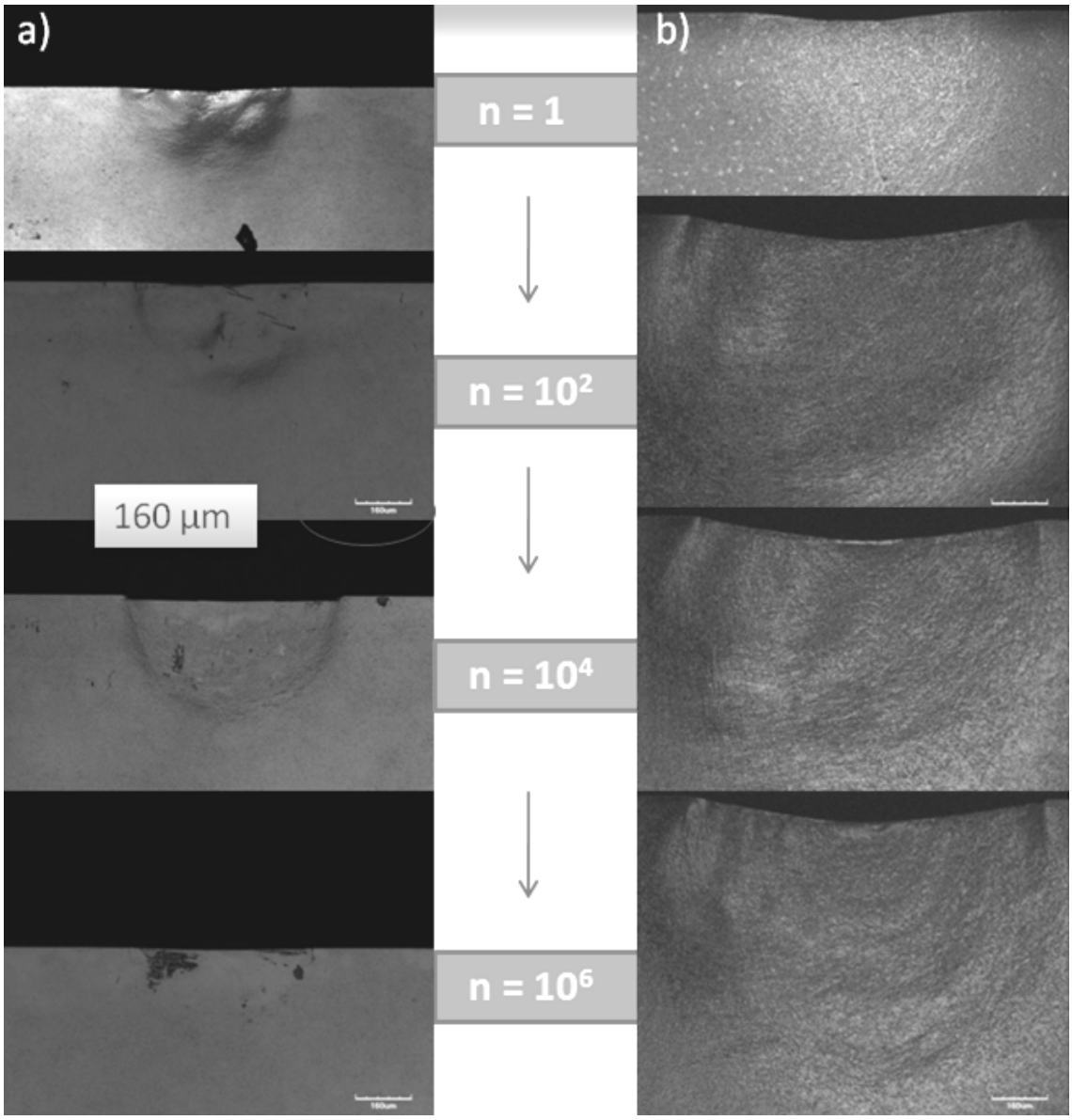

Figue 4.12. Subsurface damage evolution for cemented carbide grades C (a) and E (b) subjected to fatigue indentation loading (P_{max} =2000N) with tungsten carbide pin of radius 1.5mm.

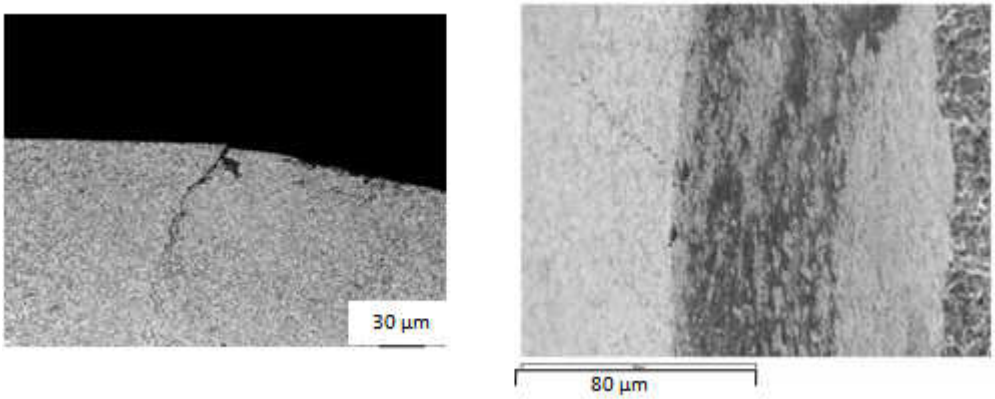

Figure 4.13. Cone crack (left) and radial crack (right) generated in grade E specimen under fatigue contact loading with P_{max} =2000N and n =10^6 cycles. Tungsten carbide pin is used with tip radius 1.5mm.

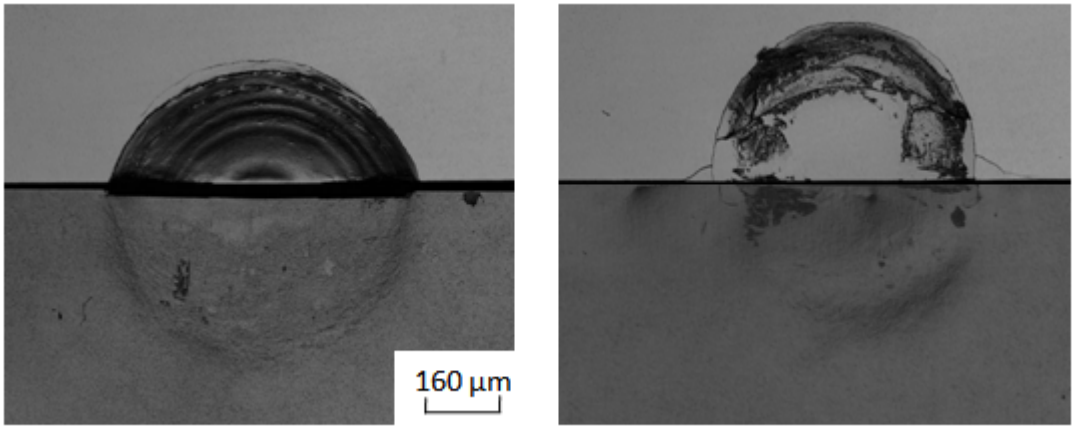

Figure 4.14. Surface (top) and section (bottom) views of contact damage in cemented carbide grade C produced by fatigue indentation with P_{max} =2000N and n= 10^4 cycles (left) and n =10^6 cycles (right). Note the presence of annular cracks and quasi-plastic deformation, as well as radial cracks in the micrograph to the right.

An interesting finding is the inverted-like cone cracks observed for the grade C specimen subjected to 10^6 cycles (Figure 4.14, right). The physics behind such cracking behavior is not clear and there is not any similar observation in the literature. It is speculated that it could be the result of the complex stress state existing from the interaction between quasi-plastic and brittle-like damage, this being relatively exclusive to very hard and relatively tough materials as hardmetal grade C.

Another interesting feature of hardmetal grade C corresponds to the propagation of a crack form the subsurface area that, according to figure 1.6, is under maximum shear stress, for a specimen subjected to fatigue contact with P_{max} =2000N and n =10^4 cycles (Figure 4.15(a)). Based on this observation, as well as on earlier studies [1], it may be stated that microcracks from the same region coalesce under cyclic loading and form macrocracks. This is completely evident in Figure 4.15(b) where extensive macrocrack formation is appreciated. It is speculated that this is indeed the seed for the appearance of radial cracks around the indentation mark. Moreover, this image also points out the potential transition of a cone crack which deviates upward and reaches the surface, into an effective radial fissure.

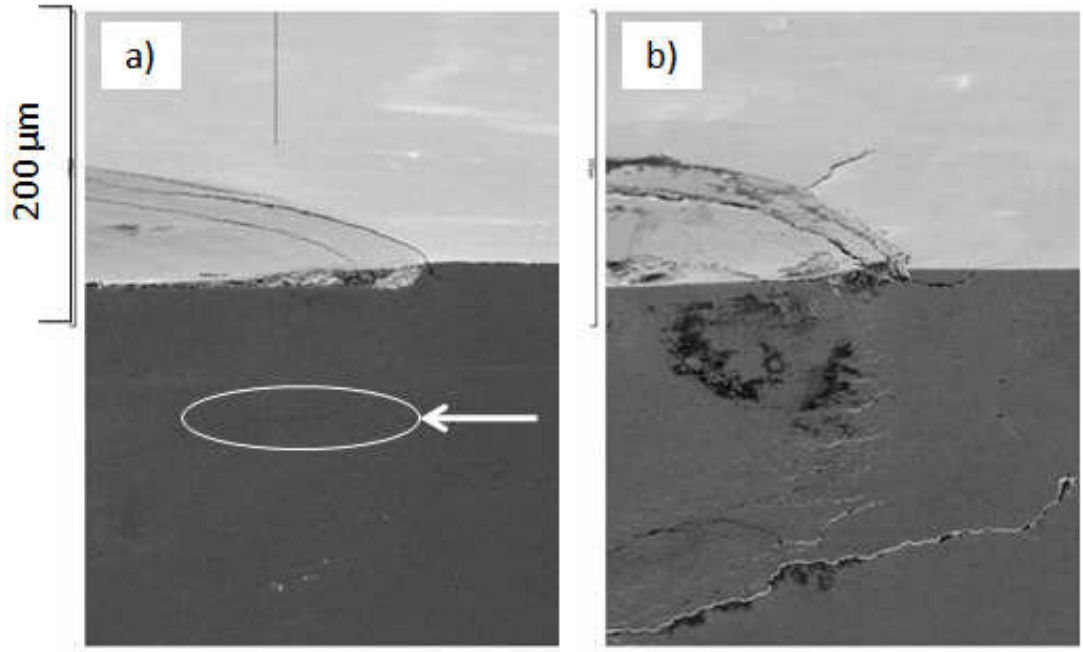

Figure 4.15. Surface (top) and section (bottom) details from cemented carbide C grade split-and-bond specimens subjected to fatigue contact loading with P_{max} =2000N and n =10^4 cycles (a) and n =10^6 cycles (b).

A corresponding study of the subsurface damage evolution of hardmetal grade E as subjected to cyclic loading is shown in Figure 4.16. As the number of cycles rises, an increasing amount of microcracks is observed, expressed as small black zones dispersed in the area beneath the contact circle, as for n =10^6. In addition, some type of cracking is manifested at the edge of the contact circle of the same indentation site, indicating the effective damage induced by cyclic indentation.

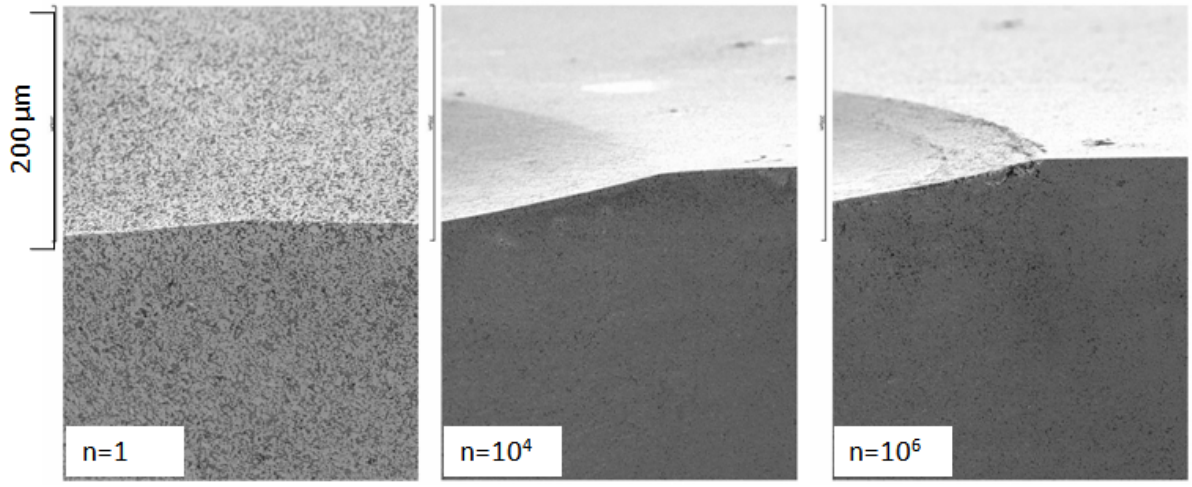

Figure 4.16. Surface (top) and section (bottom) details of E grade split-and-bond specimens subjected to fatigue contact loading with P_{max} =2000N.

Based on the observed damage, it appears as though the effects of applied spherical indentation loads under test conditions are more detrimental in the stiffer of the two hardmetal grades studied, i.e. grade C, with formation of ring cracks as well as coalescence of microcracks. However, in order to confirm or dismiss this statement, the results from the flexural tests were studied.

4.3 Fracture strength degradation

The residual fracture strength of the previously indented materials, under either monotonic or cyclic loading is shown in Figures 4.17-4.19.

In Figure 4.17, data points present experimental measurements where open symbols correspond to specimens presenting failure origins that are not associated with the indentation-induced damage. A large scatter in strength values is observed for unindented (virgin) grade C specimens. At 1750 N, it is established that some strength degradation occur, as given by strength values falling out of this scatter as well as, rupture related to indentation induced damage (closed symbols). The strength continues to decrease as contact load increases further.

Grade E specimens present strength values falling out of the initial scatter already for the applied load of 500N, where additionally, rupture is related to indentation induced damage. Further degradation is slight and occur gradually with increased load levels. Strength degradation is illustrated more clearly in Figure 4.18, where data points correspond to mean values of measured fracture strength. Vertical lines represent the standard deviation.

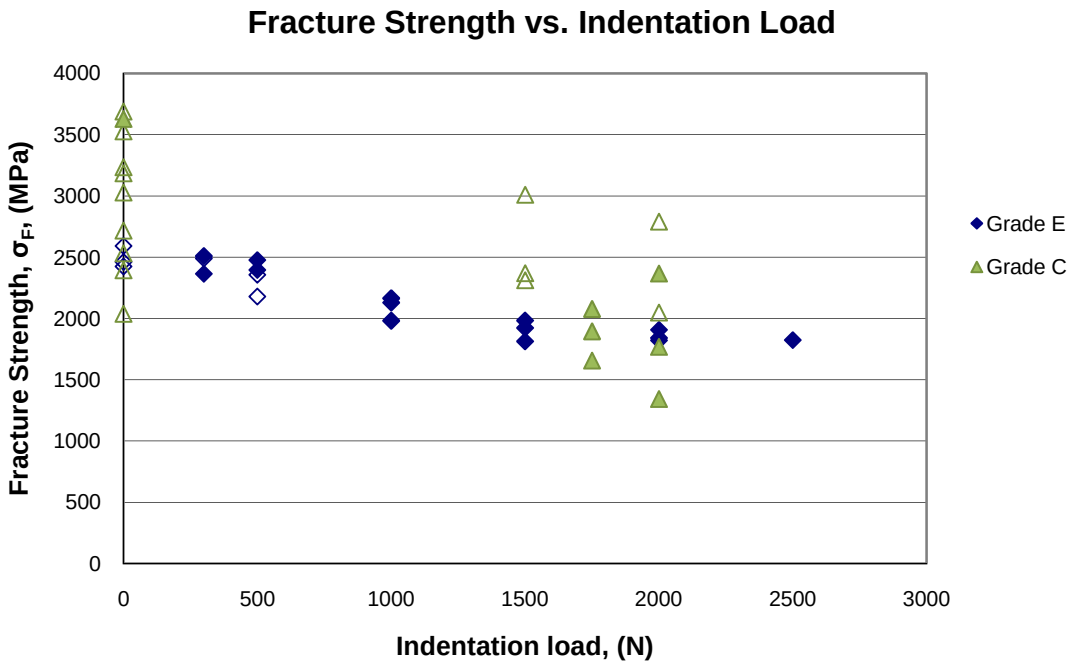

Figure 4.17. Fracture strength degradation for cemented carbide grades E and C subjected to monotonic contact loads using a tungsten carbide pin with r =1.5mm. Open symbols correspond to failure origins other than indentation.

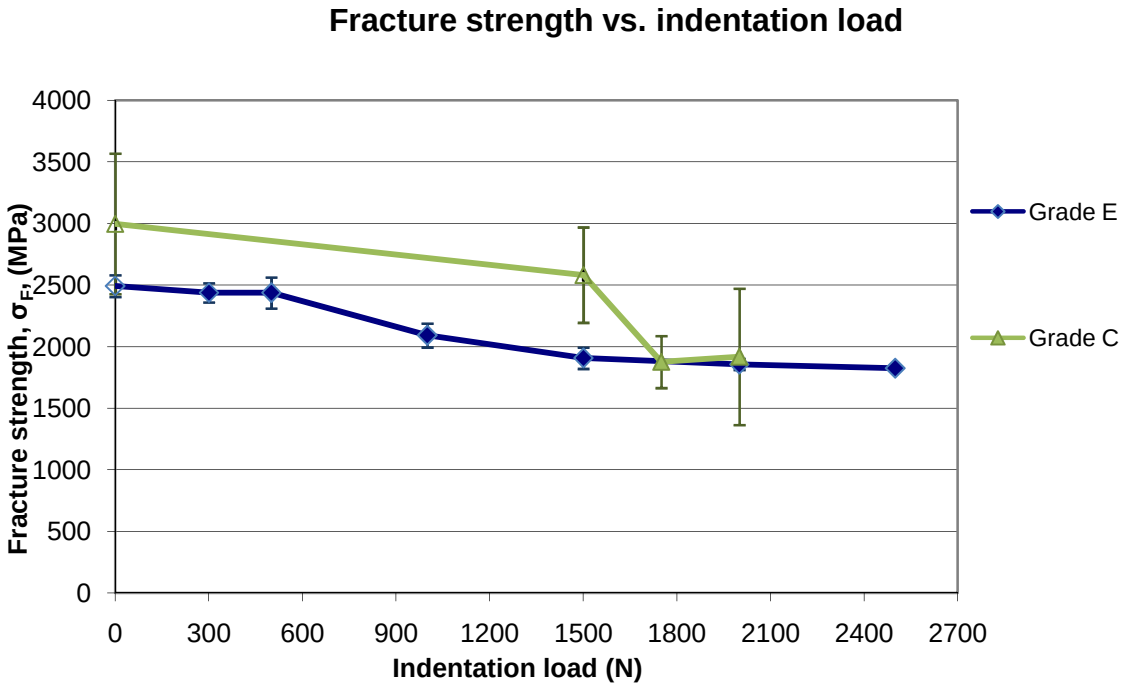

Figure 4.18. Mean values of residual mecanical strength of hardmetal grades E and C subjected to monotonic contact loads using a tungsten carbide pin of radius 1.5mm. Vertical lines indicate the standard deviation.

The residual strength of specimens previously subjected to contact fatigue is shown in Figure 4.19. Grade E specimens exposed to fatigue loads with maximum applied valued of 500N show only a slight loss in strength as the number of cycles rises up to 10^6 cycles. Increasing the maximum contact load to 2000N results in a sudden strength drop at the first contact (n =1). However, after applying a higher number of cycles the strength remains intact until n =10^6 cycles, where a slight reduction is discerned. This strength decrease is possibly a result of micro-damage buil-up in the quasi-plastic area, where it has been proved in earlier studies that microcracks coalesce upon large loads and yield radial cracks [3, 6, 13, 14]. Indeed, at n =10^6 cycles, several radial cracks are observed for hardmetal E (Figure 4.8).

Despite the slight strength decrease, cemented carbide grade E shows good fatigue properties and is to be considered relatively damage tolerant, especially when subjected to lower contact loads (500N). Nevertheless, it could be of interest to reveal its behavior at higher numbers of cycles such to assess damage evolution and its interaction with microstructure on a longer term basis.

Regarding damage induced during cyclic contact loading, grade C speciemens present a different behavior from the one described for grade E. For a relatively small number of cycles (i.e. n =1 and 10^2) strength decreases considerably, possibly as related to cone crack nucleation, reaching down to strength values half of those obtained for unindented specimens. However, once the number of cycles goes up to 10^4 cycles or beyond, residual strength recovers the levels exhibited for the unindented material.

Although such a mechanical strength may be described as unexpected, it is suspected that in grade C as cyclic deformation goes on, stress field and damage within the quasi-plastically deformed region evolves in such way that introduced damage get rather shielded. Such a shielding could be speculated to come from either effective less tensile stress state acting on induced microflaws and shallow cone cracks, or microcrack coalescence into a macrocrack, whose orientation (parallell to the surface or radial-like) may imply a less critical loading mode. In accordance, ealier studies conducted on ceramics have stated that quasi-plastic zones interact with cone cracks to neutralize the latter's effectiveness [11].

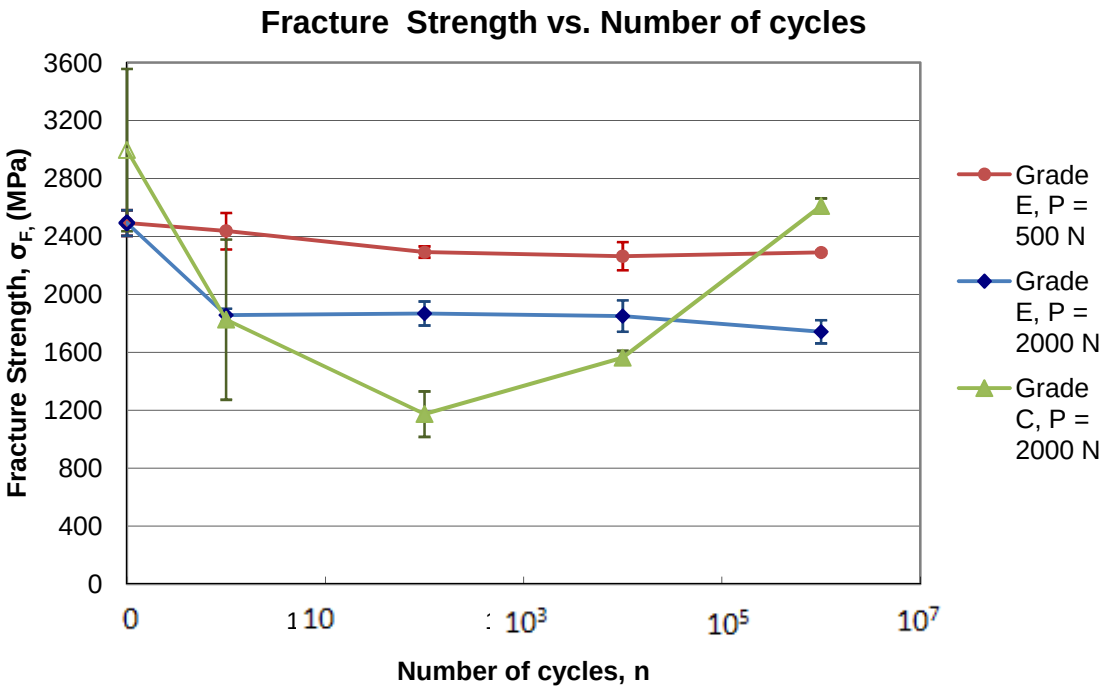

Figure 4.19. Mean values of residual strength of cemented carbide grades E and C subjected to fatigue contact loads using a tungsten carbide pin of radius 1.5mm. Vertical lines indicate the standard deviation.

Subsequent to the evaluation of residual strength, a fractographic failure analysis was conducted. Figure 4.21 show surface views of fracture sites of both hardmetals grades subjected to monotonic (n =1) and cyclic (n =10^4) loads with P_{max} =2000N. Micrographs demonstrate that failure under these conditions is due to indentation induced damage, since it can be perceived that fracture occurs at the indentation site. In grade C, fracture originates from the base of a ring crack on the edge of the contact circle. Grade E fractures along the center of the indentation impression, indicating origin in the subsurface damage zones of the material. These fracture origins can be related to the already mentioned hard and brittle nature of hardmetal grade C, and the more ductile one of grade E.

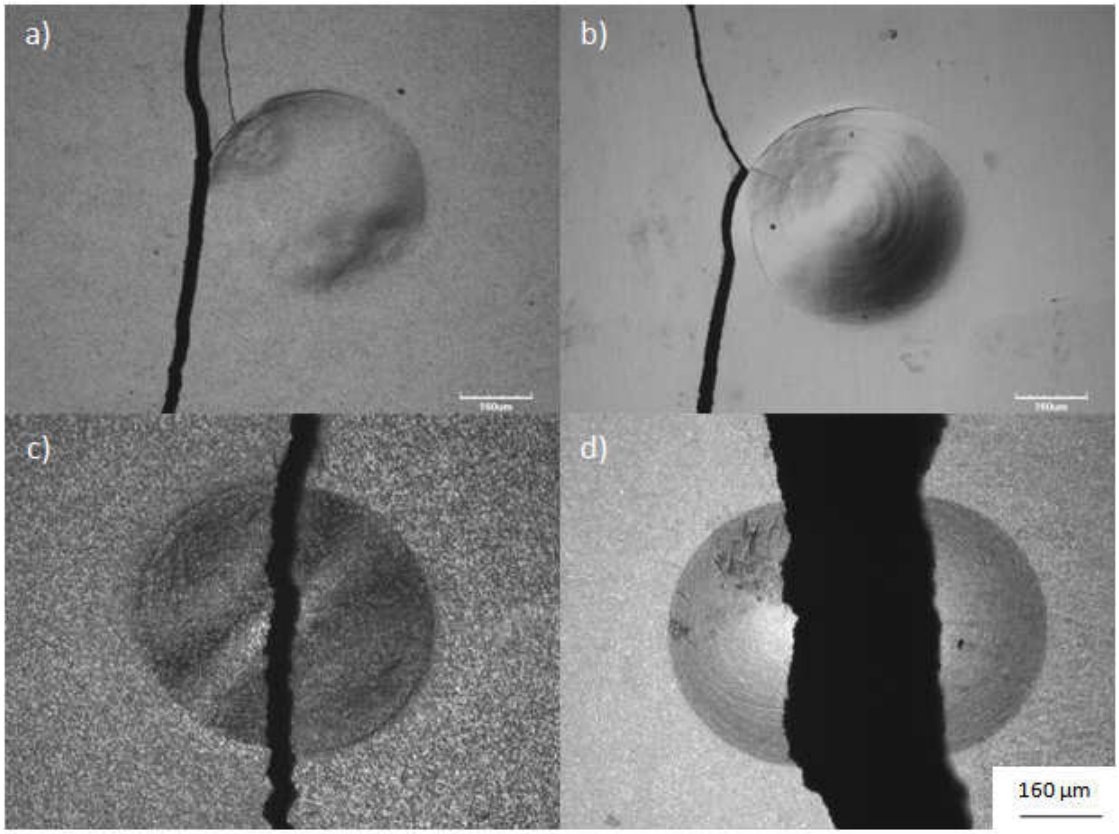

Figure 4.20. Surface views of fracture sites from four-point bending tests of previously indented cemented carbide grades C and E with indentation load P_{max} =2000N; (a) C grade, n =1 cycle (b) C grade, n =10^4 cycles, (c) E grade, n =1 cycle, (d) E grade, n =10^4 cycles.

5. Costs

Concept	Cost per unit	Amount	Subtotal (€)
Experimental equipment			
Polishing systems	10€/h	120h	1200
FRANK durometer	10€/h	1h	10
Test machine INSTRON	25€/h	160h	4000
Optical microscope	20€/h	5h	100
Optical confocal microscope	40€/h	20h	800
Scanning electron microscope (SEM)	50€/h	6h	300
Subtotal			**6410**
Laboratory materials			
Grinding discs	150 €	1	150
Polishing discs	2 €	6	12
Polishing suspension liquids	30€/l	0,5l	15
Lubricant	10€/l	3l	30
Dissolvent	2€/l	5l	10
Indentation WC-Co pins	30€	15	450
Various office materials			50
Subtotal			**717**
Specialized personnel (5 months)			
Engineer	30€/h	150h	4500
Project director	60€/h	10h	600
Laboratory technicians	25€/h	60h	1500
Subtotal			**6600**
Project total			**13727**

6. Environmental impacts

Environmental impacts of this final year research project are mainly due to the consumption of water during preparation of specimens (i.e. grinding), along with the power consumed when maintaining experimental test equipment (polish- and grind systems, durometer, servo hydraulic machines, optical and scanning electron microscopes) running. Worth mentioning is also the paper consumed when printing articles as well as this report.

7. Concluding remarks

In this project, spherical indentation tests have been used to induce damage into two hardmetal grades, such to evaluate their respective response to contact, i.e. their damage tolerance, in terms of mechanical strength, and relate this response to microstructural parameters of the material. From the findings, the following conclusions can be made:

1. The work carried out as well as the experimental findings attained indicate that methodologies well-established for evaluating damage effects on advanced ceramics may be directly implemented for studying cemented carbides.

2. It is recognized that as carbide grain size and metallic binder content decreases, hardmetals exhibit a more significant hardness and stiffness at the expense of fracture toughness. From the findings of this study, it may be added that as carbide grain size and metallic binder content increase, the hardmetal response to spherical indentation (under monotonic as well as cyclic loading) is increasingly quasi-plastic.

3. Hardmetal grade C develops both brittle cone cracks and quasi-plastic deformation in response to spherical indentation. The former initiates at elevated monotonic load levels and, in fatigue, at small number of cycles. Extended quasi-plastic deformation takes place during higher cyclic loading.

4. Hardmetal grade E presents a completely quasi-plastic response to spherical indentation, with formation of microcracks in binder as well as carbide phases, under monotonic and cyclic loading. From the quasi-plastic region, at high numbers of cycles, radial cracks are generated.

5. Materials with extensive quasi-plastic behavior experience small gradual strength degradation under increasing monotonic load levels. During cyclic loading, the degradation is slightly less significant, reflecting the relatively high damage tolerance of these materials.

6. The formation of an annular crack is suspected to cause a drop in fracture strength, explaining hereby the strength degradation of the more brittle hardmetal grade under

high monotonic load levels, and in fatigue, at small number of cycles. However, as these cracks are shallow and the material apt to quasi-plastic deformation under high cyclic loading, development of the latter may recover strength degradation by preventing crack spreading from taking place in a critical direction.

7. The results here presented for hardmetals are promising towards the implementation of methodologies based on spherical indentation as tools for assessing performance and reliability retention under service conditions for these materials. Nevertheless, effectiveness on this approach requires extensive research efforts for achieving a deeper understanding of the mechanics and mechanisms involved in the interaction among damage, microstructure and mechanical functionality for cemented carbides.

Acknowledgements

Mis más profundos agradecimientos a David Coureaux, por haberme ayudado y enseñado tanto a lo largo de este proyecto. Igual, quiero agradecer a Luis Llanes por su auyda y consejos aportados. También agradezco a todos del equipo CIEFMA, en particular a Alexey, Fransesc, Jordi, Álvaro y Giselle, por la ayuda recibida en todo momento necesario. Por ultimo, quiero darle gracias a Sato por su colaboración.

References

[1] Lawn, B. R., *"Indentation of Ceramics with Spheres; A Century after Hertz"* J. Am. Ceram. Soc. 81.8 (1998) : 1977-94

[2] González, P. M. « *Diseño de materiales multicapa resistentes al daño por contacto"*, doctor thesis, Universidad de Extremadura (Spain), 2003

[3] Zhang, H., Fang, Z. Z. *"Characterization of quasi-plastic deformation of WC-Co composite using Hertzian indentation technique*" Int. J. of Refr. Metals. & Hard Materials. 26 (2008): 106-114

[4] Lawn, B. R., Padture, N. P., Cai, H. y Guiberteau, F. *"Making Ceramics Ductile"* Science. 263 (1994) : 1114-16

[5] Didier, T. "*Evaluación de la sensibilidad al daño por contacto esférico de carburos cementados WC-Co de grano fino y ultra fino*", final year research project, Universitat Polytècnica de Catalunya (Spain), 2009

[6] Padture, N. P., Lawn, B. R. "*Contact Fatigue of a Silicon Carbide with a Heterogeneous Grain Structure*" J. Am. Ceram. Soc.78.6 (1995): 1431-38

[7] ASTM E-1876. "*Standard test method for dynamic young's modulus, shear modulus, and Poisson's ratio by impulse excitation of vibration*" Annual Book of ASTM Standards, 1997

[8] ASM international, "*Cemented Carbides*", Tool Materials, ASM Specialty Handbook, Materials Park, USA, 36-58, 1998

[9] http://www.hardmaterials.sandvik.com/ [Consulted: 15/09/09]

[10] Góez, A., Reig, B., Nordenström, H., Tarrés, E., Jiménez-Piaué, E., Llanes, L. "*Contact Damage and Residual Strength in Cemented Carbides"*

[11] Jung, Y. G., Peterson, I. M., Pajares, A., Lawn, B. R. *"Contact Damage Resistance and Strength Degradation of Glass-infiltrated Alumina and Spinel Ceramics*" J. Dent. Res 77.3 (1999): 804-814

[12] Zhang, H., Fang, Z. Z., Belnap, D. "*Quasi-Plastic Deformation of WC-Co Composites Loaded with a Spherical Indenter*" Metallurgical and Materials Transactions A 38A (2007): 552-561

[13] Abudaia, F. B., Evans, J. T., Shaw, B. A. "*Spherical indentation fatigue cracking"* Materials Science and Engineering A 291 (2005): 181-187

[14] Stuman, C. J., Field, J. E. "*The indentation of hard metals: the role of residual stresses"* J. of Materials Science 12 (1977): 215-218

[15] Aragones, T. "*Influencia de la microestructura en la resistencia a rotura y el límite de fatiga de carburos cementados*", final year research project, Universitat Polytècnica de Catalunya (Spain), 2008

[16] Jung, Y. -G., Peterson, I. M., Kim, D. K., Lawn, B. R. "Lifetime-limiting Strength Degradation from Contact Fatigue in Dental Ceramics" J. Dent. Res. 79.2 (2000): 722-731

[17] Harrison, J., Wilks, J. "*The Hertz indentation test and Auerbach's law*" J. Phys. D: Appl. Phys. 11 (1978): 73-81

[18] Callister, W. D. Jr. "*Materials Science and Engineering: An Introduction"*; John Wiley & Sons, Inc.: USA, 2003;

[19] www.allaboutcementedcarbides.com [Consulted: 15/09/09]

[20] http://www.azom.com/details.asp?ArticleID=1203 [Consulted: 15/09/09]

[21] http://www.precisionballs.com/tungsten-carbide.htm [Consulted: 16/09/09]